Journal of South American Earth Sciences 104 (2020) 102791

Contents lists available at ScienceDirect

Journal of South American Earth Sciences

journal homepage: www.elsevier.com/locate/jsames

Magmatic and tectonic fabrics in the Upper Jurassic La Hoya Pluton, North Patagonian Batholith (~43°S) as a record of the early stages of the Andean deformation

Claudia Beatriz Zaffarana [a,b,*], Bárbara Boltshauser [a,b], Víctor Ruiz González [c], Darío Leandro Orts [a,b], Samanta Serra-Varela [a,b], Carla Puigdomenech [c]

[a] Universidad Nacional de Río Negro. Instituto de Investigación en Paleobiología y Geología, Río Negro, Argentina
[b] IIPG, UNRN, Consejo Nacional de Investigaciones Científicas y Tecnológicas (CONICET), Av. Roca 1242 (R8332EXZ) General Roca, Río Negro, Argentina
[c] Consejo Nacional de Investigaciones Científicas y Técnicas (CONICET). Instituto de Geociencias Básicas, Aplicadas y Ambientales de Buenos Aires, Buenos Aires, Argentina

ARTICLE INFO

Keywords:
Laccolith
Mylonites
Anisotropy of magnetic susceptibility
Magmatic foliation
Contractional deformation
Arc magmatism

ABSTRACT

The magmatic record of the North Patagonian Batholith starts in Middle Jurassic times and rapidly grew in Early Cretaceous times, where it experienced its main building phase. Slightly after, in the Late Cretaceous, the North Patagonian fold and thrust belt experienced its first contractional deformation pulse. The La Hoya Pluton is an Upper Jurassic shallow intrusive body emplaced in the North Patagonian Andes in the proximities of the city of Esquel in Argentina. Its excellent exposures, which bear magmatic and high- and low-temperature solid-state deformation structures, are studied in this work through field, microstructural, and AMS studies. The initial shape of the pluton could be envisaged as having a geometry compatible with coalescent laccoliths, given by the presence of subhorizontal magmatic to solid-state foliations with associated E-W or N–S trending magmatic to solid-state lineations. These magmatic structures, which bear a mild solid-state overprint, were probably formed during progressive pluton cooling. Moreover, the nature of these structures suggests that the pluton cooled fast at shallow crustal levels, indicating that they are probably related to its emplacement processes that started, at least, in Late Jurassic times. Contrastingly, NW-SE and NE-SW trending high-angle subvertical fractures and low-temperature mylonitic zones with steeply plunging lineations, which are compatible with an E-W shortening direction, cut the previously formed subhorizontal magmatic structures. These compressive structures found in the La Hoya Pluton were probably developed during the Late Cretaceous main stage of contractional deformation. The contractional deformation is constrained to have happened before the intrusion of undeformed basaltic dikes crosscutting the mylonitized areas of the La Hoya Pluton. These dikes have an ^{40}Ar-^{39}Ar age in plagioclase of 42.15 ± 0.40 Ma and geochemical features typical of volcanic arcs above a subduction zone. Their geochemical signature is sensitive to the process of arc resumption after the Paleogene waning of arc activity, as it is transitional between the alkaline-like signature of Pilcaniyeu Belt (~57.8–42; Paleocene-Eocene) and the predominantly slab-derived magmas of El Maitén Belt (~37–19; Late Eocene-Early Miocene). These dikes probably formed part of the early stages of the El Maitén Belt.

1. Introduction

The North Patagonian Batholith represents a magmatic record of protracted Mesozoic-Cenozoic subduction between the South American continent and the subducting ocean floor (Munizaga et al., 1988; Pankhurst et al., 1992, 1999; Rolando et al., 2002; Rapela et al., 2005; Castro et al., 2011), characterized by a complex age distribution and episodic construction. The earliest records of the North Patagonian Batholith extend to Middle Jurassic times, and those ages, spanning a broad range of about 20 Ma between ~150 and ~170 Ma, are mostly represented in Bariloche area (41° 7.8' S, Castro et al., 2011). Batholith construction is episodic, and the distribution of ages is complex. For example, in the El Bolsón – Esquel areas (42°–43° S), granites of Middle Jurassic age are not represented, at least not with the available ages in

* Corresponding author. Universidad Nacional de Río Negro. Instituto de Investigación en Paleobiología y Geología, Río Negro, Argentina.
E-mail addresses: czaffarana@unrn.edu.ar, cbzaffarana@gmail.com (C.B. Zaffarana).

https://doi.org/10.1016/j.jsames.2020.102791
Received 12 May 2020; Received in revised form 21 July 2020; Accepted 23 July 2020
Available online 19 August 2020

the literature, which are mostly K–Ar or Rb–Sr (Fig. 1). There, the North Patagonian Batholith has ages spanning from Late Jurassic to Early Cretaceous (~161-98 Ma), although Late Cretaceous and even Eocene ages were found in the Lago Puelo and Cholila areas (~37 and ~42 Ma, Lizuaín, 1980, Fig. 1). Apart from these ages, the predominant ages of the North Patagonian Batholith in the area of Esquel and El Bolsón are Early Cretaceous, well comprised within the main building phase of the North Patagonian Batholith, which is constrained to be between 135 and 90 Ma (Pankhurst et al., 1999). Afterwards, brief periods of batholith construction were recognized at 76 Ma and c. 40 Ma, until Early Miocene times (c. 20 Ma) when another intense magmatic outburst took place (Pankhurst et al., 1999).

Before the construction of the North Patagonian Batholith, a short-lived NNW-SSE striking calc-alkaline batholith of Early Jurassic age was intruded. It was baptized as Sub-Cordilleran Patagonian Batholith (Gordon and Ort, 1993) or Subcordilleran Plutonic Belt (Haller et al., 1999). The intrusion of the Subcordilleran belt represented the activity of the subduction zone during with the Gondwana breakup stage (Rapela et al., 2005). Granites of these ages are found in the El Bolsón – Esquel area, near Leleque and Epuyén, and to the east, in the broken foreland area, c. 100 km to the east of Trevelin (Fig. 1).

Going back into time, intrusive rocks of Paleozoic age also crop out in the North Patagonian Andes and in the broken foreland area (Fig. 1), representing remnants of old magmatic arcs and collisional processes (Pankhurst et al., 2006 and references therein, see Fig. 1). In relation to what has been exposed above, intrusive rocks of different ages overlap in the North Patagonian Andes and the broken foreland area between 42° and 43° S. In this manner, the area enclosed in Fig. 1 appears as of great interest to investigate in detail the geochronological aspects of this arc-related magmatism.

The focus of this contribution is to study the deformation of the La Hoya Pluton, an igneous body which had been considered as part of the Subcordilleran Plutonic Belt, with a K–Ar whole rock age of 174 ± 20 Ma (Toubes and Spikermann, 1973). However, a recently obtained ^{40}A-^{39}Ar stepwise age in hornblende of 161.9 ± 0.46 Ma, permitted to assign it to the early stages of the North Patagonian Batholith (Fig. 1; Boltshauser et al., 2019). In this work we perform a structural and anisotropy of magnetic susceptibility (AMS) study of this pluton to constrain the

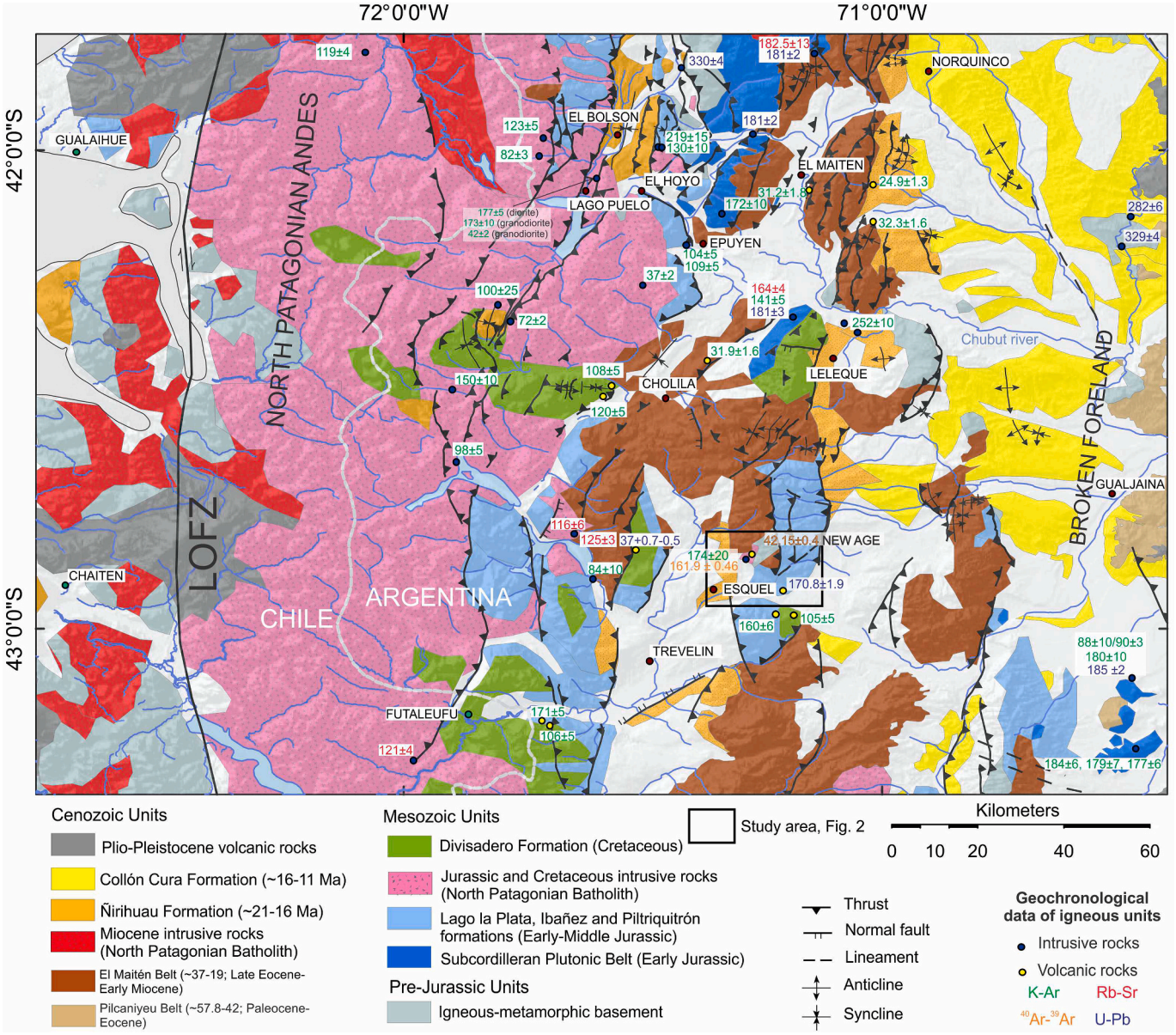

Fig. 1. Regional geological map of the North Patagonian Andes, modified from Lizuaín and Viera (2010), Orts et al. (2012) and Echaurren et al. (2017). The compiled ages of intrusive and volcanic rocks are listed in Table 1-Appendix. LOFZ: Liquiñe-Ofqui fault zone.

history of the early stages of Andean deformation in the southern end of the Esquel range (Fig. 1). It is known that plutons are considered as deformation markers, and AMS studies have proved to be an excellent tool to track weak deformation, such as the one usually present in granitic rocks (e.g., Archanjo et al., 1995, 2002; Saint Blanquat and Tikoff, 1997; Ferré and Améglio, 2000; McNulty et al., 2000; Neves et al., 2003; Žák et al., 2005; D'Eramo et al., 2006; Stevenson, 2009; Somoza et al., 2015; Olivier et al., 2015; Nédélec and Bouchez, 2015; Zaffarana et al., 2017). AMS studies have relevance in determination of magmatic lineations, which generally are hard to measure in the field or the laboratory using the microscope. Tectonic interpretations of the susceptibility ellipsoid rely on that it corresponds to the strain ellipsoid (e.g., Jelinek, 1981; Borradaile and Jackson, 2010). The three principal axes of the anisotropy of the magnetic susceptibility ellipsoid ($K_1 > K_2 > K_3$) define, when $K_1 > K_2$, a magnetic lineation parallel to K_1, and a magnetic foliation (when $K_2 > K_3$) as the plane containing K_1 and K_2, with K_3 being the pole to foliation. The typical relationship between the anisotropy of the magnetic susceptibility ellipsoid and petrofabric shows the magnetic lineation parallel to the structural lineation (stretching or flow) and the magnetic foliation parallel to the structural foliation (flattening or flow). Sometimes this relationship may be obliterated by superposition of fabrics or by a particular mineral phase (e.g., Rochette et al., 1992, 1999; Borradaile and Henry, 1997). Determining the minerals that dominate the magnetic signal is important when analyzing AMS data.

The mapping of fabrics in plutons includes their classification in magmatic and solid-state fabrics, mostly following the criteria of Paterson et al. (1998). In magmatic fabrics, grain boundaries are mostly straight, and quartz shows only weak undulose extinction. In the sub-magmatic state described by Paterson et al. (1989) and Bouchez et al. (1992), quartz grains have moderate undulose extinction, with the formation of some incipient deformation bands, although no changes in the shape of the grains is apparent. Biotite may show some bending and feldspars are not strained, although myrmekites develop locally. Solid-state deformation fabrics comprise high-temperature and low-temperature solid-state deformation fabrics. High-temperature deformation fabrics develop in the range of ~500–700 °C, that is, near-solidus to subsolidus temperatures (Paterson et al., 1998). Primary microstructures diagnostic of this type of fabric are chessboard subgrain pattern in quartz (above 700 °C, Blumenfeld et al., 1986; Mainprice et al., 1986), local development of myrmekites (Passchier and Trouw, 2005) and abundant flame perthites in K-feldspar (Pryer, 1993). Other microstructures of this stage are the inversion of orthoclase to microcline (Eggleton and Buseck, 1980) and undulose extinction in biotite. Strong post-emplacement solid-state deformation, where recrystallization of most minerals into small grains is common, though not complete, show subgrains which may be organized in bands. Microstructures include subgrains in quartz and incipient bulging and microfracturing in feldspars. These processes occur at relatively low to medium temperature conditions (300–500 °C) and/or fast strain rates (Passchier and Trouw, 2005; Vernon, 2000). Mylonites have S fabrics and are rich in porphyroclasts which consist of variably rounded plagioclase and orthoclase with textures indicating both brittle and crystal-plastic behavior. These include fractures and micro-faults filled with mylonite matrix minerals, undulatory extinction, bent grains and twins, glide twinning, subgrains, and weakly to moderately developed, winged, recrystallization mantles.

When applying the above-mentioned criteria, the La Hoya Pluton has magmatic and tectonic fabrics, acquired during pluton cooling (magmatic and high- and low-temperature conditions) and after, in low-temperature conditions. The age of deformation can be constrained to have occurred before the intrusion of the undeformed basaltic dikes which intrude the La Hoya Pluton. These dikes, which had remained undocumented in the literature, until now, are dated by the ^{40}Ar-^{39}Ar stepwise method as Eocene.

2. Geological framework

The La Hoya Pluton is a 25 km^2 stock intruded near 43° S, in the southern end of the Esquel range in the North Patagonian Andes (Figs. 1 and 2). It is composed of two main facies, monzogranites and granodiorites, together with minor gabbroic and quartz-monzodioritic stocks and dikes. This pluton was dated in 161.9 ± 0.46 Ma by ^{40}Ar-^{39}Ar stepwise heating in hornblende crystals; thus, this age allows its classification as the part of the early stages of the North Patagonian Batholith (Boltshauser et al., 2019). This pluton had only a previous K–Ar age of 174 ± 20 Ma (Toubes and Spikermann, 1973, Fig. 1).

The host rocks of the La Hoya Pluton are the late Paleozoic Esquel and Valle Chico formations (Cazau, 1972; González Bonorino, 1992). These units crop out in the Esquel range and in the Cerro Excursión area (Figs. 1 and 2). The Early Jurassic Piltriquitrón Formation (González Bonorino, 1974; Lizuaín, 1980) and the Early-Middle Jurassic Lago La Plata Formation (Echaurren et al., 2017; Zaffarana et al., 2020) also host La Hoya Pluton. The Lago La Plata Formation has U–Pb dating in zircon age of 170.8 Ma ± 1.9 Ma in the southern end of the Esquel range (Blesa, 2004, Fig. 1). Cretaceous volcanism is represented by the Divisadero Group (Late Lower Cretaceous; Haller and Lapido, 1982; Echaurren et al., 2017).

The intrusion of the Patagonian Batholith took place in Middle Jurassic-Cenozoic times, with most of its outcrops located west of the study area (Fig. 1, Bruce et al., 1991; Pankhurst et al., 1992; Pankhurst and Hervé, 1994; Rolando et al., 2002; Castro et al., 2011). As was mentioned in the introduction, the construction of the North Patagonian Batholith was complex and occurred in different stages, and batholith construction times are generally correlated with periods of orthogonal convergence (Pankhurst et al., 1999). The construction of the Patagonian fold and thrust belt occurred in several stages as well; the early phase of construction occurred in Late Cretaceous times (Orts et al., 2012; Echaurren et al., 2016, 2017), slightly postdating the main construction phase of the North Patagonian Batholith.

Paleocene-Eocene volcanism is represented by the ~57.8–42 Ma Pilcaniyeu Belt, also known in the literature as Huitrera Formation (Feruglio, 1949; Ramos et al., 1982; Rapela et al., 1988). The Pilcaniyeu Belt comprises a bimodal volcanic association interbedded with continental deposits (Rapela et al., 1984, 1988) that crops out between 40° and 44°S in the broken foreland zone, towards the east of the area of study (Fig. 1). This volcanism was ascribed to the interruption of the subduction zone took at 50–52 Ma until ~37 Ma due to the collision of the Farallón-Aluk ridge with the South American border (Aragón et al., 2011, 2013; Iannelli et al., 2020; Fernández Paz et al., 2018). Although the volcanism of the Pilcaniyeu Belt has slab-derived geochemical features, their alkaline-like features are robust (Iannelli et al., 2017).

After the waning of arc volcanism represented by the Pilcaniyeu Belt, the magmatic activity in the magmatic arc restarted, represented by the Ventana Formation (González Bonorino, 1974) that forms part of the El Maitén Belt (~37-19 Ma; Rapela et al., 1988; Iannelli et al., 2017; Fernández Paz et al. 2018, 2019; 2020, Fig. 1). The El Maitén Belt is a Late Eocene-Early Miocene volcano-sedimentary sequence formed by basaltic and andesitic lavas together with minor pyroclastic rocks, interbedded with marine deposits in its upper part (González Bonorino, 1974; Dalla Salda et al., 1981; Ramos et al., 1982; Rapela et al., 1988; Bechis et al., 2014). The volcanic rocks within the El Maitén Belt are calc-alkaline, with a change to tholeiitic compositions toward the upper part of the unit (Rapela et al., 1984, 1988; Litvak et al., 2014; Iannelli et al., 2017; Fernández Paz et al. 2018, 2019; 2020).

Since Late Eocene times, an extensional period took place in the Southern Central Andes (Charrier et al., 2002; Godoy et al., 1999; Jordan et al., 2001; Radic et al., 2002), coevally with the extrusion of the El Maitén Belt. Synextensional geochemical and structural features were described for the volcanic rocks of this belt (Rapela et al., 1988; Giacosa and Heredia, 2004; Bechis and Cristallini, 2006; Aragón et al., 2011; Bechis et al., 2014; Fernández Paz et al., 2018, 2019; 2020).

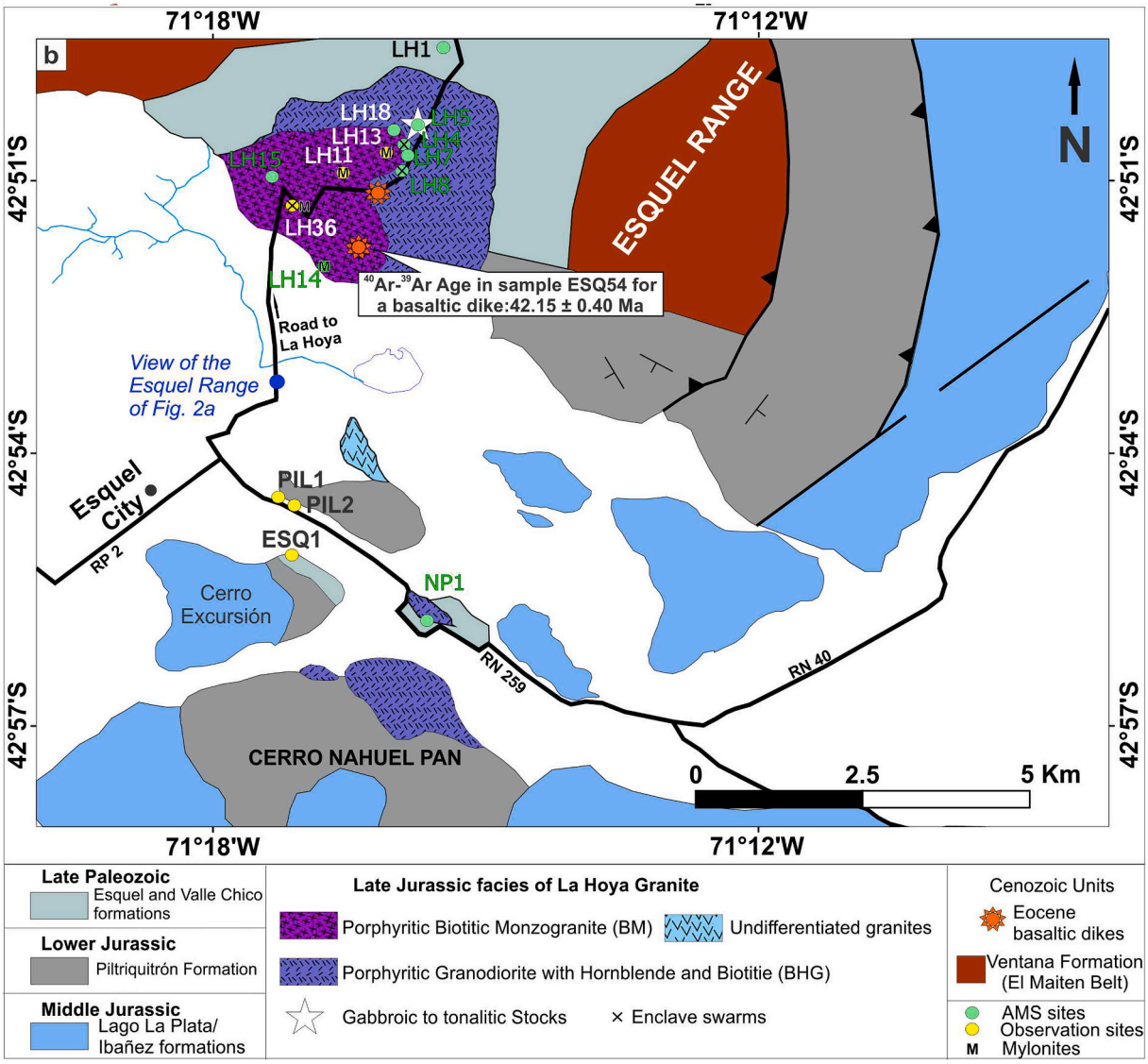

Fig. 2. Geological map of the La Hoya Pluton and its host rock. Modified after Lizuaín (2010) and Boltshauser et al. (2019). Exact location of the sites with structural observations: ESQ1: 42.918 °S and 71.285 °W, PIL1: 42.907 °S and 71.287 °W, PIL2: 42.909 °S and 71.284 °W, LH11: 42.851 °S and 71.276 °W, LH13: 42.844 °S and 71.265 °W and LH36: 42.856 °S and 71.285 °W.

In Miocene times, a new contractional deformation stage occurred (Giacosa and Heredia, 2004; Orts et al., 2012, 2015; Bechis et al., 2014; Encinas et al., 2013, 2014; Echaurren et al., 2016, 2017) producing the tectonic inversion of the El Maitén depocenters (Orts et al., 2012, 2015; Echaurren et al., 2016; Fernández Paz et al., 2018). The Miocene contractional deformation phase was at least partly coeval with the Miocene suites of the North Patagonian Batholith (e.g., Pankhurst et al., 1999).

3. Methods

Microstructural observations were performed on a collection of 50 thin sections, with those from outcrops having visible tectonic foliation being orientated according to planar and, whenever possible, linear structures observed in the field. Nine AMS sites were collected, with a total of 116 specimens (see Table 1). Sites were distributed along a road that traverses the central part of the pluton covering an overall vertical relief of ~900 m (Fig. 2). Access to the highest outcrops of the pluton is difficult due to the high relief of the area (Fig. 3a), therefore the observations were made in key areas of the pluton, for example, enclave swarm areas, and sectors showing mylonitic deformation.

Anisotropy of the magnetic susceptibility measurements were performed by using a MFK1-B Kappabridge susceptibilimeter. Anisotropy of the magnetic susceptibility ellipsoids (with principal axes $K_1 > K_2 > K_3$) were calculated from a minimum of five specimens per site using matrix averaging routines (Jelinek, 1978, 1981) with the programs ANISOFT 4.2 (Chadima and Jelinek, 2008).

Hysteresis curves and isothermal remanent magnetization-backfield analyses were performed with an applied field up to 1.8 T using a Lakeshore 7404 Vibrating Sample Magnetometer (VSM) at the Laboratorio de Aplicaciones Efecto Mössbauer y Magnetismo (LAEMM) from the Departamento de Física of the Universidad Nacional de La Plata, Argentina. The nominal value of bulk magnetic susceptibility may give an idea of the minerals that control the magnetic susceptibility. Bouchez (2000) proposed that when magnetic susceptibility is higher than 4×10^{-4} SI, the magnetic susceptibility is mainly controlled by ferromagnetic minerals (mainly magnetite), and the rock can be classified as "ferromagnetic", with multidomain (MD) magnetite dominating the bulk susceptibility. However, in the samples that contain only magnetite, the diagram of Day et al. (1977), constructed with the hysteresis

Table 1
AMS sites of the La Hoya Pluton and the Esquel/Valle Chico formations. Lat. and Long. are site latitude and longitude. Fabric records if the samples bear magmatic "M" or low-temperature solid-state deformation "S". N is the number of samples used in statistics. Km=(K_1+K_2+K_3)/3 is the mean magnetic susceptibility (SI units). L is the magnetic lineation (K_1/K_3); F is the magnetic foliation (K_2/K_3); P is the degree of anisotropy (Jelinek, 1981); T=(lnF − lnL)/(lnF + lnL) is the Jelinek's parameter (Jelinek, 1981). K_1, K_2 and K_3 are mean AMS eigenvectors which represent the maximum, intermediate and minimum susceptibility intensities, respectively. Dec, declination in degrees; Inc, inclination in degrees; C1a and C1b are the semiangles of the major and minor axes of the 95% confidence ellipse, respectively, calculated by the bootstrap method.

Site	Lat (°S)	Lon (°W)	subsite	fabric type	Rock type	Samples	N	Kaver	Std. Error	Pjmean	Tmean	Lmean	Fmean	Pmean
LH5	−42.84	−71.263	all samples	M + S	Gabbros	H18, H19	12	8.29E-02	3.51E-02	1.024	−0.407	1.016	1.007	1.023
	−42.84	−71.263	LH5 prolate	S	Gabbros and qtz-monzodiorites	H18	6	1.02E-01	1.31E-02	1.035	−0.599	1.027	1.007	1.033
NP1	−42.93	−71.261	no subsites	M + S	Granodiorites	E4, E5, E6, E7, E8	26	5.24E-02	1.71E-02	1.022	−0.293	1.014	1.008	1.021
LH4	−42.844	−71.265	no subsites	M + S	Granodiorites	H12, H13, H19	12	0.0302	1.89E-02	1.028	−0.426	1.019	1.008	1.027
LH7	−42.846	−71.264	no subsites	M + S	Granodiorites	H23, H25	9	1.82E-02	1.44E-02	1.048	−0.072	1.026	1.022	1.048
LH8	−42.848	−71.265	all samples	M + S	Granodiorites	H28, H29	13	1.41E-02	6.41E-03	1.047	0.053	1.022	1.024	1.047
	−42.848	−71.265	LH8 tectonic	S	Granodiorites		6	1.73E-02	2.84E-03	1.066	0.335	1.021	1.043	1.065
LH18	−42.841	−71.266	all samples	M + S	Monzogranites	H63, H66	12	1.20E-02	3.79E-03	1.032	−0.02	1.016	1.015	1.032
	−42.841	−71.266	LH18 tectonic	S	Monzogranites		5	0.0128	3.49E-03	1.048	−0.19	1.028	1.019	1.048
LH15	−42.852	−71.285	no subsites	M	Monzogranites	H54, H55	13	0.00322	1.44E-03	1.048	0.794	1.004	1.039	1.044
LH14	−42.866	−71.279	all samples	S	Monzogranites	H47, H48, H49, H52, H53	13	8.53E-03	7.71E-03	1.017	0.11	1.008	1.009	1.017
	−42.866	−71.279	LH14 tectonic	S	Monzogranites		6	1.02E-02	8.09E-03	1.029	0.186	1.012	1.017	1.029
LH1	−42.826	−71.255	no subsites	–	Esquel/Valle Chico formation (host rocks)	H1, H3	6	0.000411	1.012	1.019	−0.408	1.013	1.005	1.018

Site	subsite	fabric type	Rock type	Samples	N	K1d	K1i	C1a	C1b	K2d	K2i	C2a	C2b	K3d	K3i	C3a	C3b
LH5	all samples	M + S	Gabbros	H18, H19	12	81.1	59.3	25.4	13.3	233.6	27.8	39.5	14.2	330.1	12	36.8	10.5
	LH5 prolate	S	Gabbros and qtz-monzodiorites	H18	6	68.8	66.4	22	10.3	259	23.3	43.4	12	167.4	3.7	41.5	9.7
NP1	no subsites	M + S	Granodiorites	E4, E5,E6, E7,E8	26	26.2	8.2	18.6	11.7	285.8	51.2	46.5	16.8	122.6	37.6	46.3	12.1
LH4	no subsites	M + S	Granodiorites	H12, H13, H19	12	84.9	1.3	14.5	12.4	175.9	37	22.3	13.3	353.1	53	22.5	12.3
LH7	no subsites	M + S	Granodiorites	H23, H25	9	270.5	14	19.4	10.8	180.2	1.3	18.3	12.2	84.9	75.9	18.3	8.5
LH8	all samples	M + S	Granodiorites	H28, H29	13	285.5	22.9	18	12.7	22.4	15.9	29.7	14.4	144.2	61.6	28.2	12.6
	LH8 tectonic	S	Granodiorites		6	283.7	16.5	17.2	9.6	20.7	22.5	26.6	6.9	160.5	61.6	22.5	9.2
LH18	all samples	M + S	Monzogranites	H63, H66	12	199.6	7.6	31.8	6.7	104.4	33.8	44.7	15.8	300.7	55.1	44.6	15.8
	LH18 tectonic	S	Monzogranites		5	199.7	8.9	15.7	1	107.3	2.3	52.7	2.3	319.2	72.4	53	11
LH15	no subsites	M	Monzogranites	H54, H55	13	182.9	12.2	37.1	6.7	92.2	2.9	37.8	6.2	349	77.5	11.8	5.9
LH14	all samples	M + S	Monzogranites	H47, H48, H49,H52, H53	13	298.4	56.7	23.1	17.2	74.4	25.3	49.2	18.5	174.4	20.2	50.5	10.1
	LH14 tectonic	S	Monzogranites		6	304.9	58.5	14.1	12.6	76.3	22.1	42.9	12	175.4	21.3	43.7	5.6
LH1	no subsites	–	Esquel/Valle Chico formation (host rocks)	H1, H3	6	130.7	20.7	11.3	6.9	35.9	12.6	39.4	7.8	276.5	65.4	39.2	4.2

parameters such as coercive force (Hc), saturation magnetization (Ms) and remanent magnetization (Mr), together with the remanent coercive force (Hcr) taken from backfield measurements, was constructed to estimate the domain state of magnetite.

Sample ESQ54 from the basaltic dikes intruding the La Hoya Pluton was analyzed by the ^{40}Ar-^{39}Ar method at the University of Nevada, Las Vegas (USA) (see Table 2-Appendix and Supplementary Material). In addition, whole-rock geochemical data of samples ESQ51 and ESQ54 of the basaltic dikes were performed at the Acme Analytical Laboratories (Acmelabs), Vancouver, Canada. Samples were analyzed with the 4B code procedure. ICP-OES determined major and minor elements, and trace elements (Ba, Cs, Ga, Hf, Nb, Rb, Sr, Ta, Th, U, V, Zr, Y and REEs) by ICP-MS. In both cases, fusion with lithium metaborate/tetraborate flux was conducted upon completion of rock powder dissolution. Data

Table 2
Whole-rock geochemical data. Major oxides in wt % and trace elements in ppm.

Sample	ESQ51	ESQ54
Latitude (S) and longitude (W)	42°51′5.1" - 71°16′35.8″	42°51′19.6" - 71°16′57.6″
SiO_2	56.85	57.11
TiO_2	0.99	0.96
Al_2O_3	18.53	18.46
FeO	6.39	6.45
Fe_2O_3	–	–
MnO	0.105	0.117
MgO	3.92	3.70
CaO	7.51	7.53
Na_2O	4.06	4.003
K_2O	1.32	1.34
P_2O_5	0.28	0.29
Cr_2O_3	0.004	0.004
Total	100	100
LOI	3.3	4.1
U	0.8	0.7
Th	3.7	3.2
Zr	166.4	163.3
Hf	4.3	4.8
Ta	1.1	0.7
Nb	8.4	8.3
Y	20.6	20.4
Ba	352	447
Sr	493.6	1470.8
Rb	27.4	27.6
Ni	31	37
La	18.8	13.4
Ce	39.2	36.4
Pr	5.48	5.03
Nd	21.8	20
Sm	4.72	4.41
Eu	1.5	1.22
Gd	4.28	4.03
Tb	0.71	0.63
Dy	4.09	3.65
Ho	0.84	0.8
Er	2.24	2.28
Tm	0.38	0.33
Yb	2.29	2
Lu	0.35	0.33
Sc	16	15
Ga	19.4	18.1
FeO_t/MgO	1.62	1.74
Ba/La	18.72	33.35
Ba/Ta	320	638.57
La/Sm	3.98	3.03
Sm/Yb	2.06	2.20
Eu/Eu*	1.01	0.88
La/Yb	8.20	6.7
Th/Hf	0.86	0.84
Ta/Th	0.29	0.21
Ta/Hf	0.25	0.18
La/Ta	17.09	19.14
Mg#	52.28	50.58
Nb/Zr	0.05	0.05
Ba/Nb	41.90	53.85

reduction was carried out using Igpetools (https://www.ugr.es/~fbea/fbea/Software.html) in STATA programming language (Statacorp, 2014).

4. Results

4.1. Field observations and microstructures

The La Hoya Pluton is a concentrically zoned igneous body that covers approximately 25 km^2, with an excellent exposure (Fig. 3a). It has a normal zonation pattern, with granodiorites and gabbro-tonalites in the outer region, and monzogranites in the inner region. The presence of myarolitic cavities, granophyric textures, and general fine-grained to porphyritic textures confirm shallow emplacement conditions for this pluton, which intrudes volcanic rocks of nearly the same age (Early Jurassic Piltriquitrón and Early-Middle Jurassic Lago La Plata formations) and low-grade Paleozoic metamorphic rocks (Esquel and Valle Chico formations, Figs. 1 and 2).

In the Cerro Excursión area (ESQ1 site in Fig. 2), the Late Paleozoic strata constitute an alternating series of sandstones and siltstones with an S_1 parallel to bedding (S_0), and later this foliation (S_1 and S_0) is deformed by a disjunctive crenulation cleavage (S_2) (Fig. 3b and c). In the area near Esquel city (sites PIL1 and PIL2 in Fig. 2) the Piltriquitrón Formation is formed by a subvertical NE-SW alternation of sandstones and mudstones, together with some matrix-supported breccias (Fig. 3d–f).

The primary fabric of the La Hoya Pluton is magmatic, although superimposed low-temperature deformation is practically ubiquitous in the whole unit, as well as propylitic hydrothermal alteration in different degrees (Fig. 4).

Petrographic observations on samples from the 8 AMS sites and from other different observation sites (sites LH11, LH13, LH36, ESQ1, PIL1 and PIL2, their location is given in the caption of Fig. 2) were made to gain insights into the petrofabric of these rocks. Microstructures within the La Hoya Pluton formed before full-crystallization to low-temperature solid-state deformation conditions. We classified microtextures in two categories: M and S fabrics. Fabric type M is magmatic and sub-magmatic, formed previously to full-crystallization. Solid-state deformation fabrics S comprise high-temperature and low-temperature solid-state deformation fabrics, including mylonitic rocks.

In general, in the La Hoya Pluton fabrics which started in the magmatic or sub-magmatic stage and evolved in solid-state conditions with progressive cooling of the pluton (M + S), are more common than pure M fabrics. The sole example of a pure M fabric was recorded in site LH15, where the monzogranites show undeformed granophyric texture (Fig. 4a). Magmatic fabrics are recorded in the enclave swarm areas (sites LH4, LH8 and LH36), because the enclaves usually record the original magmatic foliation, at least at outcrop scale. However, when seen under the microscope, nearly all the samples analyzed from the La Hoya Pluton show the typical association of high-temperature deformation microstructures, given by myrmekites, microcline instead of orthoclase and chessboard texture in quartz (Fig. 4b and c). When observed, low-temperature solid-state deformation is incipient in most samples from the La Hoya Pluton, as aggregates of small quartz and feldspar subgrains that tend to be isolated while many mineral boundaries remain straight (Fig. 4b, c, f, i, j, k, l). However, in some samples, such as in the mylonites of site LH14, quartz and feldspar subgrains that are interconnected in shear bands (Fig. 4e). Solid-state deformation in the La Hoya Pluton seems to be aided by or related to hydrothermal alteration, as solid-state deformation microtextures are present in the samples where mafic minerals are replaced by chlorite, plagioclase is altered to sericite and K-feldspar is replaced by clays (Fig. 4b–c, f-l). Quartz frequently shows polygonal grain boundaries due to static recrystallization or to textural coarsening (Higgins, 2011, Fig. 4g and h).

The hydrothermal alteration of the La Hoya Pluton has been explained in two ways: either as part of the outer propylitic halo of the Esquel low-sulfidation epithermal deposit, composed of chlorite, zoisite, illite, calcite and quartz (Blesa, 2004); or as part of the regional low-grade metamorphism that affected the Esquel region, which produced a very similar mineral assemblage (Aguirre et al., 1997; Vattuone et al., 2001; Massaferro, 2000). Our observations of the intense alteration in the deformed plutonic rocks indicate fluid circulation during mylonitization, independently of the regional extension of this hydrothermal alteration.

Mylonitic strips are frequent, generally subvertical, formed in fine-to medium-grained monzogranites from La Hoya Pluton, and have NW-SE strike (N320°, site LH13 and N350°, site LH11), or NE-SW strike (N41° strike in site LH36; Fig. 1b; Fig. 5a–i). Undeformed basaltic dikes intrude the mylonites of site LH13 (Fig. 5a). Mylonites are a few decameter broad zones of inhomogeneous deformation consisting of numerous

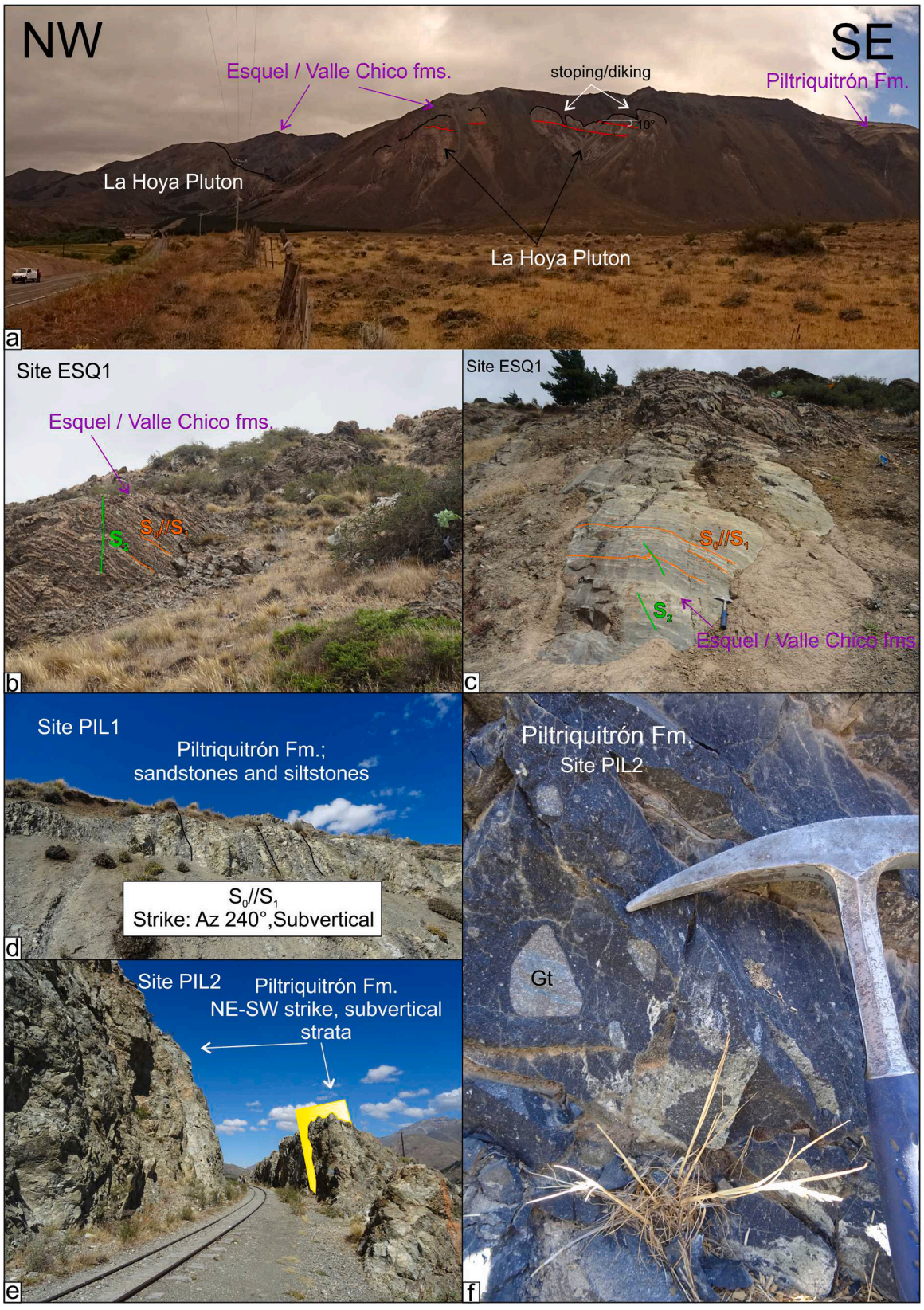

Fig. 3. Outcrops of the La Hoya Pluton and its host rocks. a) Regional view from the point signaled in Fig. 2 of the Esquel range, with the La Hoya Pluton showing a subhorizontal magmatic foliation (dipping gently (10°) to the SE), a flat roof, and some stopping or diking processes at the top of the intrusion. b-c) Esquel and Valle Chico formations near the Cerro Excursión area (site ESQ1 in Fig. 2). S_0 compositional foliation given by sandstones and siltstones parallel to the S_1 surface; they are cut by S_2 axial planes d) Piltriquitrón Formation at site PIL1 in Fig. 2 with a compositional foliation S_0 parallel to the S_1 foliation, the sequence is defined by an alternating series of sandstones and siltstones, subvertical and with a strike of Az. 240°. e) Piltriquitrón Formation at site PIL2 (Fig. 2), showing the same attitude than in site PIL1. f) Detail of the matrix-supported breccias of site PIL2, having clasts of granitic composition.

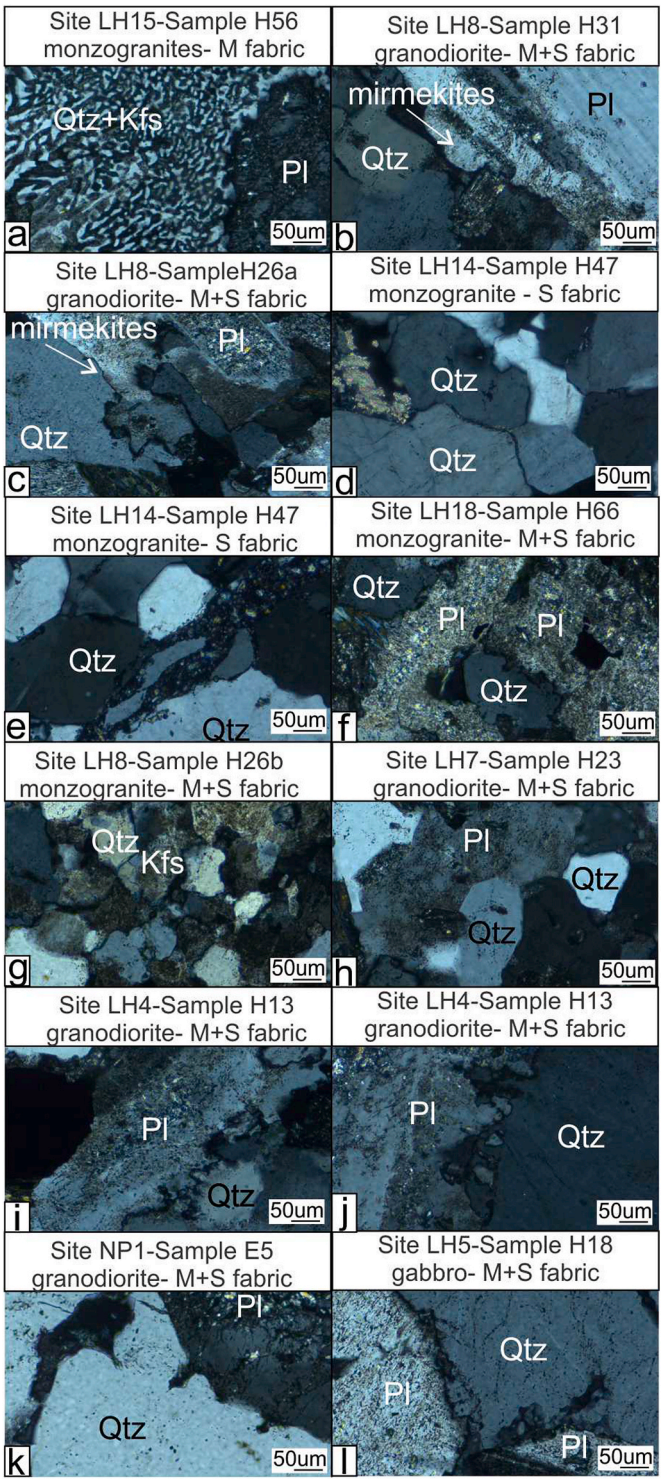

(caption on next column)

Fig. 4. Petrographic features of the AMS sites of the La Hoya Pluton. a) Magmatic texture at site LH15, where the granophyric texture is unaltered. b) and c) High-temperature solid-state deformation at site LH8, where myrmekitic lobes are observed in plagioclase, as well as low-temperature deformation given by quartz and feldspar subgrains. d) Detail of polygonal grain boundaries in quartz in a sample from site LH14. e) Subgrains of quartz and feldspar organized in bands in the mylonites from site LH14. Polygonal grain boudaries in the quartz grains as well. f) Quartz and plagioclase with modified grain boundaries by bulging and dynamic recrystallization in site LH18. g) Modified magmatic fabric in site LH8, where plagioclase, K-feldspar and quartz form subgrains due to dynamic recrystallization. h) Polygonal grain boundaries in quartz and plagicoclase in site LH7. i-j) Quartz and plagioclase with strongly modified grain boundaries due to dynamic recrystallization in site LH4. k) Indented grain boundaries in site NP1 due to grain boundary migration processes. l) Low-temperature grain boundary migration and dynamic recrystallization in plagioclase and quartz in sample LH5. Mineral abbreviations after Whitney and Evans (2010).

centimetric to metric wide, steeply dipping, mylonitic shears separating wider zones of relatively undeformed monzogranites (Fig. 5b and c). The main mylonitic foliation consists of submillimetric thick alternating layers and lenses of polycrystalline quartz ribbons, very fine-grained feldspar-rich layers, and biotite-rich (±magnetite) layers. Mineral lineations are steeply plunging in site LH13 (Fig. 5d, f), but lineation plunges 65° towards the north in site LH11 (Fig. 5g). Shear sense could be determined, in some cases, due to the presence of Riedel shear faults. For example, in the case of the mylonites of site LH36, an reverse sense of shear was observed (Fig. 5e).

A 1m wide fault zone is observed at site LH11 with an attitude of 215°/63° whose reverse kinematics was determined by Riedel shear zones (Fig. 5i). This fault zone, marked in green in Fig. 5h and i, crosscuts two different previous sets of structures. The first one is defined by the planes of subhorizontal attitude, which are cut, in turn, by the second set of structures given by high-angle fracture zones (marked in blue in Fig. 5h), which are related with the mylonites described above (scheme in Fig. 5g). At site LH11, the subhorizontal structures are recorded by M + S fabrics, and the second set of structures, the vertical ones, bear microstructures of S type, recording only microstructures of low-temperature solid-state conditions (Fig. 5h).

Sites LH4 and LH8 from the granodiorites belong to two enclave swarm areas (Fig. 6a–c). In site LH8, the enclaves appear flattened (Fig. 6a), defining a shallowly dipping magmatic foliation plane. The whole enclave swarm is traversed by late aplitic veins rich in quartz, which in sectors have a brecciated texture (Fig. 6a). In site LH4, the enclaves are more rounded (Fig. 6b). In both sites, the enclaves show diffuse borders with their host and are rich in acicular amphibole (Fig. 6c).

4.2. Mean susceptibility and minerals controlling the AMS fabric of the La Hoya pluton

Mean susceptibility in the La Hoya Pluton is 8.29 x10^{-2} SI for the gabbros, 2.87 x 10^{-02} for the granodiorites, and 7.92 x 10^{-3} for the monzogranites. The sandstones of the Esquel Fm. have a mean Km of 4.11 x 10^{-4} SI (Table 1). Bulk susceptibility values in most of the samples of the La Hoya Pluton, higher than 4 x 10^{-4} SI, suggest that the AMS signal is dominated by magnetite. This is corroborated in the hysteresis loops of Fig. 7a and b, in the IRM and backfield curves of Fig. 7c, and d. However, some interesting things can be remarked, such as the influence of paramagnetic minerals in the monzogranites represented by sample H5, which show a tendency towards no saturation in the hysteresis loop of Fig. 7a, but a remanence controlled by magnetite (shown by the saturation tendency in the IRM and backfield curves, Fig. 7c and d). Hematite is present in two samples, in the monzogranites represented by sample H8 and in the gabbros and quartz-monzodiorites represented by sample H22. Those samples tend to no saturation in the hysteresis loop

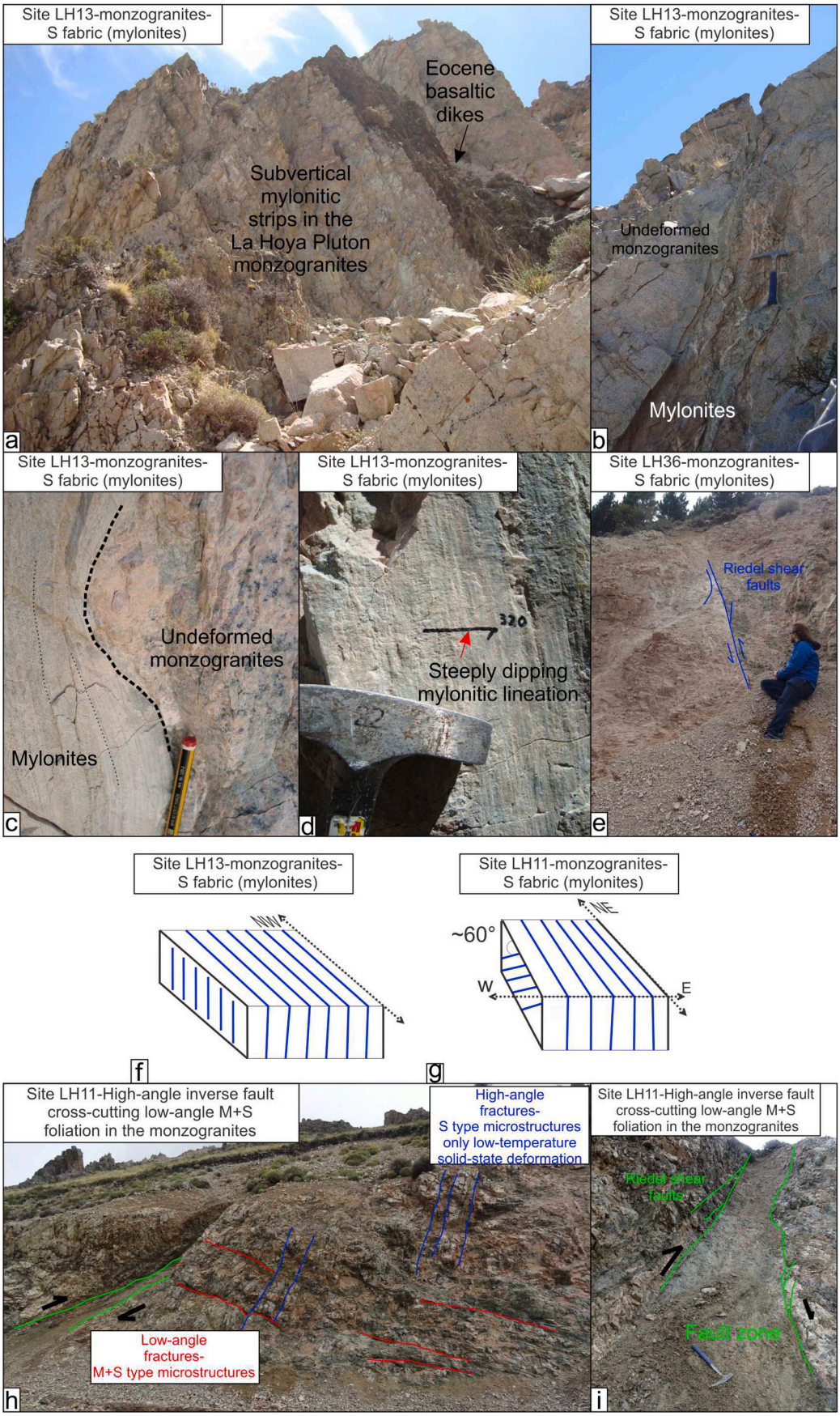

Fig. 5. Mylonitic rocks in La Hoya Pluton. a) Subvertical mylonitic rocks in the monzogranites at site LH13 intruded by undeformed Eocene basaltic dikes. b) Detail of the subvertical mylonites of site LH13 bounded by undeformed biotitic monzogranites. c) Detail of the sinuous contact between the mylonitized and the relatively undeformed monzogranite at site LH13. d) Steeply dipping stretching lineation at site LH13. e) Reverse high-angle fault in the monzogranites at site LH36, the reverse sense of shear was inferred from the Riedel shear faults f) and g) schemes of the mylonites of site LH13 (f) and LH11 (g). h) Roadcut showing shallowly dipping faults (marked in red) being cut by high-angle faults (marked in blue), and both sets of structures are cut by areverse fault (green). i) Detail of the reverse fault shown in h, with Riedel shear faults showing the inverse sense of shear. (For interpretation of the references to colour in this figure legend, the reader is referred to the Web version of this article.)

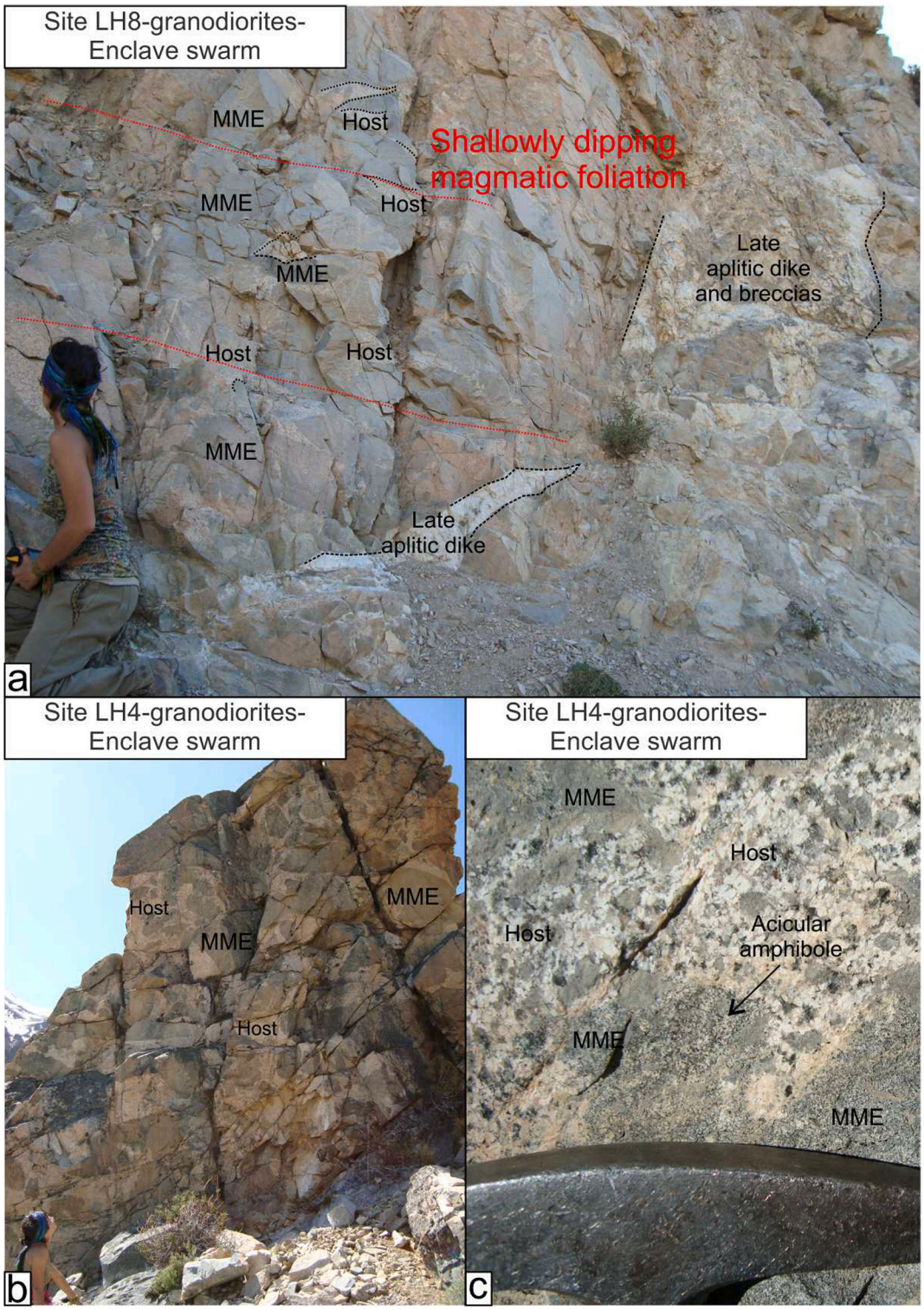

Fig. 6. Enclave swarms in La Hoya Pluton. a) At site LH8 showing the shallowly dipping magmatic foliation defined by the elongated mafic microgranular enclaves (MME). Late aplitic dikes and breccias rich in quartz and K-feldspar intrude the enclave swarm. b) Enclave swarm developed in the granodiorites at site LH4, the orientation of the magmatic foliation is not so evident in this site. c) Detail of the acicular amphibole in the enclaves of site LH4.

of Fig. 7a, and in the IRM and backfield curves as well (Fig. 7c and d).

In the diagram of Day et al. (1977) all samples showed that they are composed of multidomain to pseudo-single domain magnetite (MD and PSD magnetite, respectively, Fig. 7e), allowing for standard interpretation of results. Therefore, the magnetic lineation is the maximum eigenvector (K_1) of the magnetic susceptibility tensor, and the magnetic foliation pole is the minimum eigenvector (K_3).

4.3. Anisotropy of magnetic susceptibility data and correlation with field measurements

AMS orientations agree well with field measurements. A description of the AMS data from La Hoya Pluton and its host rock is presented in the following paragraphs, ordered by lithology.

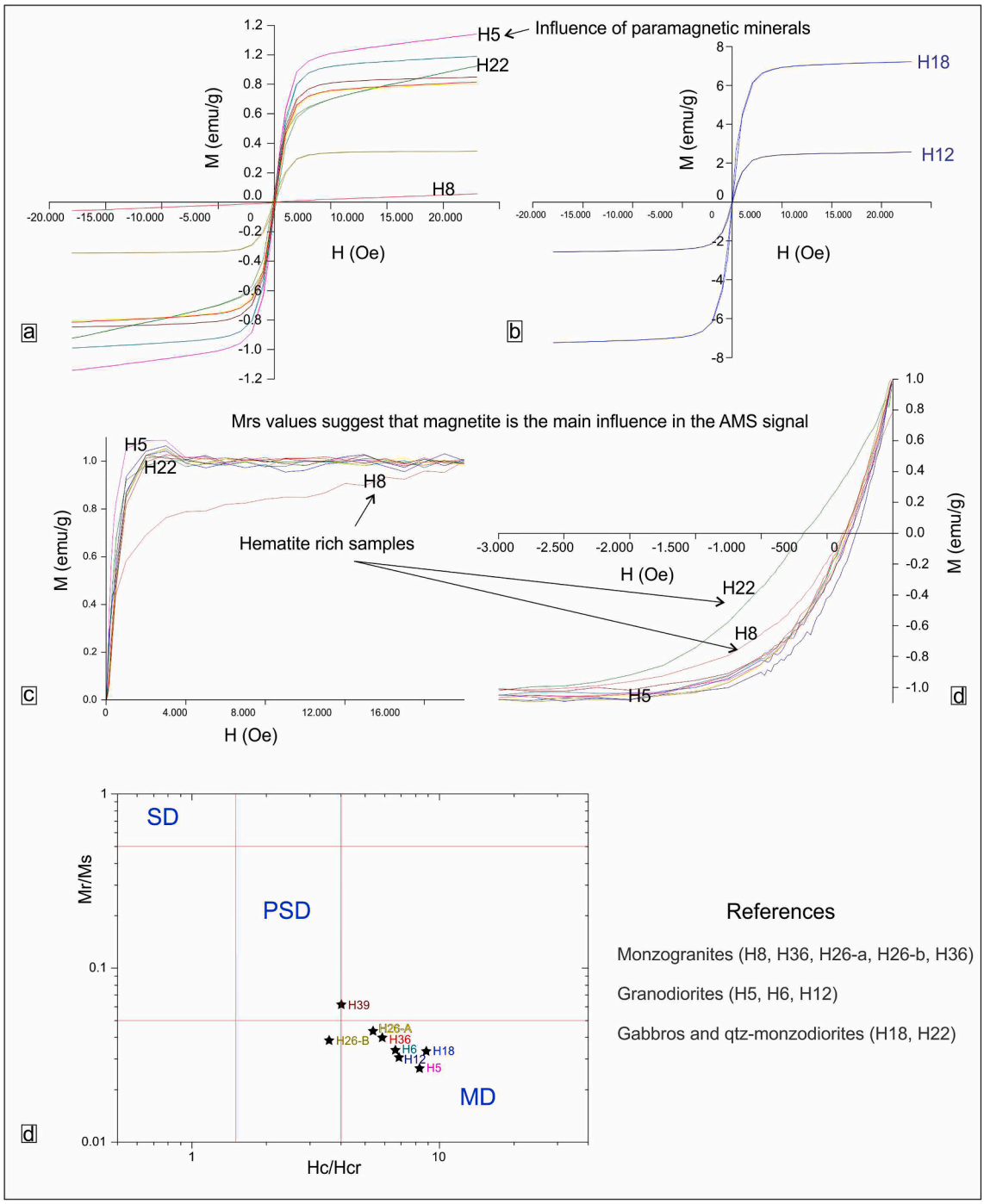

Fig. 7. Rock magnetic studies performed in some samples of the La Hoya Pluton. a) and b) Hysteresis cycles c) IRM curves d) Backfield curves e) Diagram of Day et al. (1977) for the samples whose magnetic signal is governed by magnetite. The different facies of the La Hoya Pluton have multidomain (MD) to pseudosingle (PSD) domain magnetite. Samples H22 and H8, which have hematite, were not plotted in this diagram.

4.3.1. Monzogranites

A magmatic fabric is recognized in the monzogranites of site LH15 (Figs. 4a and 8a). There, P and Km are not correlated, so the deformation of the rocks controls the moderate anisotropy degree (Pj = 1.048; Table 1, Fig. 8a). The AMS ellipsoids of the monzogranites of this site are mostly oblate, as T = 0.794, and the magmatic foliation is better defined than the magmatic lineation. The subhorizontal magmatic foliation belongs to a highly differentiated monzogranite with an undeformed granophyric texture.

In the two remaining monzogranite sites, LH18 (Figs. 4f and 8b) and LH14 (Fig. 4d and e; 8c), the fabrics are magmatic and tectonic, as deformation started in the magmatic state, and progressed in solid-state conditions. In these sites, the specimens showing the highest P values can be separated into a different ellipsoid with S fabrics. No direct correlation is seen in the P vs. Km graph, suggesting that magnetite content is not responsible for the increasing deformation degree of the rocks. The M + S and the filtered S ellipsoids from both sites are triaxial, as T values are low; thus, magmatic and tectonic foliations and lineations are well defined. The filtered S-type ellipsoids are coaxial with the foliations and lineations found in the M + S-type ellipsoids (Fig. 8b and c).

In site LH18 from the monzogranites, the tectonic foliation is

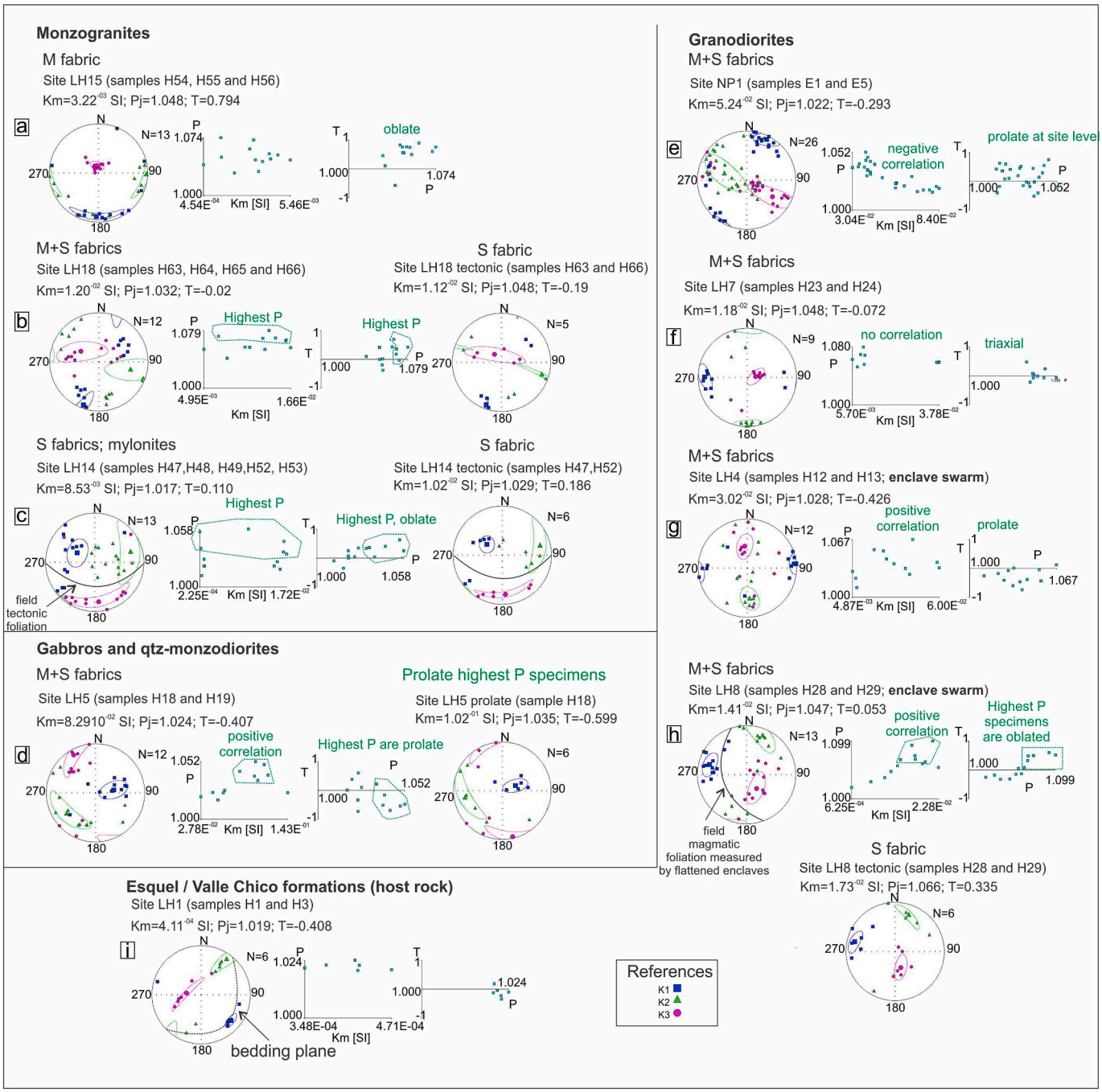

Fig. 8. AMS ellipsoid for the 9 sites of the La Hoya Pluton and the Esquel/Valle Chico formations. The P vs. Km and T vs. P graphs for the individual samples are also shown. Equal area projection in geographic coordinate system.

subhorizontal, with a shallowly plunging ~ N–S lineation. In contrast, in the mylonites from site LH14 from the monzogranites, the tectonic foliation is subvertical, with a steeply dipping lineation. In site LH14, the tectonic foliation determined with the ASM method partly coincides with the strike of the brittle structures seen in the field, where the foliation has an E-W strike and a dip of 60° towards the south.

4.3.2. *Gabbros, monzodiorites and granodiorites*

In the gabbroic and monzodioritic site LH5, fabrics are described as M + S-type because quartz shows incipient dynamic recrystallization (Fig. 4l). In this site, the specimens showing the highest P values are those which are more prolate ("site LH5 prolate", Table 1, Fig. 8d). The magnetic ellipsoid of this site is prolate, and the individual samples are strongly prolate as well. However, the positive correlation of P and Km suggests that magnetite is responsible for the increasing P of the individual samples of the site (Fig. 8d), in concordance with the hysteresis cycle of these rocks (Fig. 7a), which shows that magnetite is responsible for the AMS signal. Therefore, the better-defined lineation found in the samples with higher P is not interpreted as of tectonic origin, because the positive correlation of Km and P suggests that P is controlled by magnetite instead of by fabric strength. In site LH5 from the gabbros and quartz-monzodiorites, the better-defined lineation, given by the specimens recording the highest P-value that are more strongly prolate, is subvertical (Fig. 8d).

In the granodiorites, four sites were determined (Table 1; Fig. 8e–h). All sites, NP1, LH7 LH4, and LH8, have M + S-type fabrics, as

deformation started in the magmatic and continued in the tectonic stage (Fig. 4b and c and 4h-k).

In site NP1, a negative correlation between Km and P is seen (Fig. 8e), and in site LH7, no correlation between Km and Pj is found (Fig. 8f) suggesting that the anisotropy degree is governed by the intensity of deformation. However, in both sites, specimens with higher P are mostly triaxial, as P and T do not show any correlation. Therefore, fabrics obtained with and without filtering the specimens with the highest P values are mostly the same, and magnetic foliations and lineations are well defined. Site NP1 from the granodiorites has a subvertical foliation plane of NNE-SSE strike, and a NNE trending, shallowly plunging lineation. In the field, a conspicuous tectonic foliation plane of NE-SW strike and subvertical inclination was seen, which coincides with the orientation of the magnetic foliation seen with the AMS method.

In contrast, in site LH4, taken from an enclave swarm area (Fig. 6b and c), there is a positive correlation between Km and P, thus suggesting that magnetite is governing the anisotropy degree of these rocks (Fig. 8g). The AMS ellipsoid is mostly prolate, both at the specimen and at the site level; therefore, the magnetic lineation is better defined than the magnetic foliation plane.

Site LH8 from the granodiorites belongs to an enclave swarm (Fig. 6a), and there, too, a positive correlation between Km and P is found (Fig. 8h). The fact that the specimens with higher P are more strongly oblate, instead of prolate, suggests that the ductile deformation of the rocks controls the anisotropy degree, as the mafic microgranular enclaves seen in the field are oblate as well (Fig. 6a). The high-temperature deformation microstructures seen in this site, given by myrmekites and inversion of orthoclase to microcline and chessboard quartz (Fig. 4b and c), suggest that this deformation started in the magmatic, and lasted throughout the post-magmatic stage. The plane defined by the solid-state deformation is shallowly dipping, and the horizontal lineation has an E-W strike. In the field, the attitude of the plane defined by the oblate enclaves was taken; it bears an attitude of 170°/50°, partly coinciding with the data obtained with the AMS method.

Site LH7 from the granodiorites, together with sites LH4 and LH8 from enclave swarm areas, have subhorizontal to shallowly dipping foliation planes, and E-W trending, shallowly plunging lineations (Fig. 8g-h). It is essential to mention that lineation was better defined in site LH4 (Fig. 8g), where it is horizontal, with a well-defined E-W strike.

4.3.3. Host rock: Esquel and Valle Chico formations

The host rocks belonging to the Esquel and Valle Chico formations were drilled in site LH1 (Fig. 2), where they are represented by massive metasandstones rich in quartz and bearing an S0 parallel to an S1 low-grade metamorphic foliation of Az 75° strike and a shallow dip (10°-30° towards the SE). The magnetic susceptibility of these rocks is low, is 4.11×10^{-4} SI (Fig. 8i). The magnetic ellipsoid is triaxial, and no direct relationship was found between the anisotropy degree and mean susceptibility values of the individual samples. The magnetic foliation coincides with the bedding plane measured in the field. However, K1 is well grouped, indicating pencil structures associated to an early deformation stage (Ramsay and Huber, 1983; Parés and van der Pluijm, 2002).

4.4. ^{40}Ar-^{39}Ar age and geochemistry of the intruding basaltic dikes

Subvertical basaltic dikes with sharp boundaries intrude the La Hoya Pluton (Fig. 4a; 9a), and they are not affected by the solid-state deformation affecting the La Hoya Pluton, nor by the regional propylitic alteration. The field relations and the freshness of the basaltic dikes would suggest a recent age of emplacement. These dikes crop out with only one direction exposed, so it was impossible to measure the strike in many of them. They have variable widths, ranging from 1 to 10 m. They are dark brown rocks, with porphyritic texture (20% of clinopyroxene phenocrysts). Cataphyllary erosion is a common feature of these intrusives (Fig. 9b). The groundmass presents intergranular to subophytic texture; it is composed of plagioclase (50%), clinopyroxene (35%), olivine is replaced by iddingsite (10%) and opaque minerals (5%) (Fig. 9c). In contrast with all the plutonic facies of the La Hoya Pluton, these basaltic dikes do not show traces of the hydrothermal alteration that affects the whole pluton.

The somewhat U-shaped age spectrum of sample ESQ54, and lower initial and final radiogenic yields are compatible with the presence of excess argon in the sample (Fig. 9d). As no isochron or plateau age could be obtained, the minimum age (42.15 ± 0.40 Ma, Eocene) on the age spectrum (see Table 2-Appendix) should be considered as the age of the sample, due to the excess argon assumption which would render the age to be older than its true age.

Geochemical results from samples ESQ51 and ESQ54 show 56–57% SiO_2, 1.32–1.34% K_2O, 4.03–4.06% Na_2O, and an Mg # of between 50 and 52 (anhydrous base, loss on ignition (LOI) contents between 3.3 and 4.1; Table 2). On the TAS diagram, rocks are classified as dacites, close to andesites (Le Bas et al., 1986, Fig. 10a).

Chondrite-normalized rare earth element (REE) patterns of the samples are moderately enriched in light REEs and have a flat REEs slope ($(La/Sm)_N$ = 1.89–2.48and $(La/Yb)_N$ = 4.55–5.57; Table 2; Fig. 10b). Samples do not show negative Eu anomalies (Eu/Eu* = 0.88–1.01; Table 2, Fig. 10b). The Primordial Mantle normalized pattern of the samples bears enrichment in Rb, Sr, K, Ba, Th, U, La and Ce, and depletion in Nb, Ta, Ti, Dy, Y, and Lu (Fig. 10c), showing a remarkable Ta–Nb depletion. Trace element ratios of Ba/Nb > 40, Ta/Hf > 0.15 and La/Nb > 1 are typical of subduction environments, although the La/Ta < 25 ratio is more typical of intraplate settings (Table 2).

5. Discussion

5.1. Comparison between the eocene basaltic dikes from esquel and the Pilcaniyeu and El Maitén belts

The Eocene age of the basaltic dikes at Esquel of 42.15 ± 0.40 Ma places them between the Paleocene-Eocene Pilcaniyeu Belt (Rapela et al., 1988; Aragón et al., 2011; Iannelli et al., 2017), and the Late Eocene-Early Miocene El Maitén Belt (Rapela et al., 1988; Iannelli et al., 2017; Fernández Paz et al., 2018). As excess argon was inferred to be present in the sample, producing an age anomalously old, we believe that it is more probable that the basaltic dikes of Esquel belong to the early stages of the El Maitén Belt, than to the final stages of the Pilcaniyeu Belt. It must be considered that the basal deposits of the El Maitén belt were dated in 37 + 0.7–0.5 Ma at only 20–25 km west of the study area by Fernández Paz et al. (2018) (Fig. 1).

An integration of the geochemical features of the Eocene dikes within a more regional analysis that includes the Pilcaniyeu and the El Maitén belts is helpful to contextualize these newly found rocks from Esquel. The analysis shown here suggests that the Eocene dikes from Esquel show geochemical features transitional between both volcanic belts. In the multielemental diagram of Fig. 10c, they have Nb and Ta throughs, like the El Maitén Belt. They are subalkaline in the TAS diagram, like the El Maitén Belt (Fig. 10a), but they have La/Ta<25 like the Pilcaniyeu Belt, which is typical of intraplate environments (Fig. 10d). In the Ba/La vs. Th/La, in the Nb/Zr vs. Ba/Nb and the Th/Hf vs. Ta/Hf diagrams, the Eocene dikes from Esquel show intermediate characteristics between both belts (Fig. 10e–g). We conclude that these dikes have characteristics compatible with subduction-derived magmas, but they have some features typical of extensional magmatism as well.

5.2. Deformation in the La Hoya pluton

The La Hoya intrusive body is an upper crustal, flattened pluton whose geometry can be envisaged as a combination of laccolith bodies which, with successive snapshots, evolve towards a piston-like bysmalith (a cylindrical, fault-bounded, piston-like laccolith, Horsman et al.,

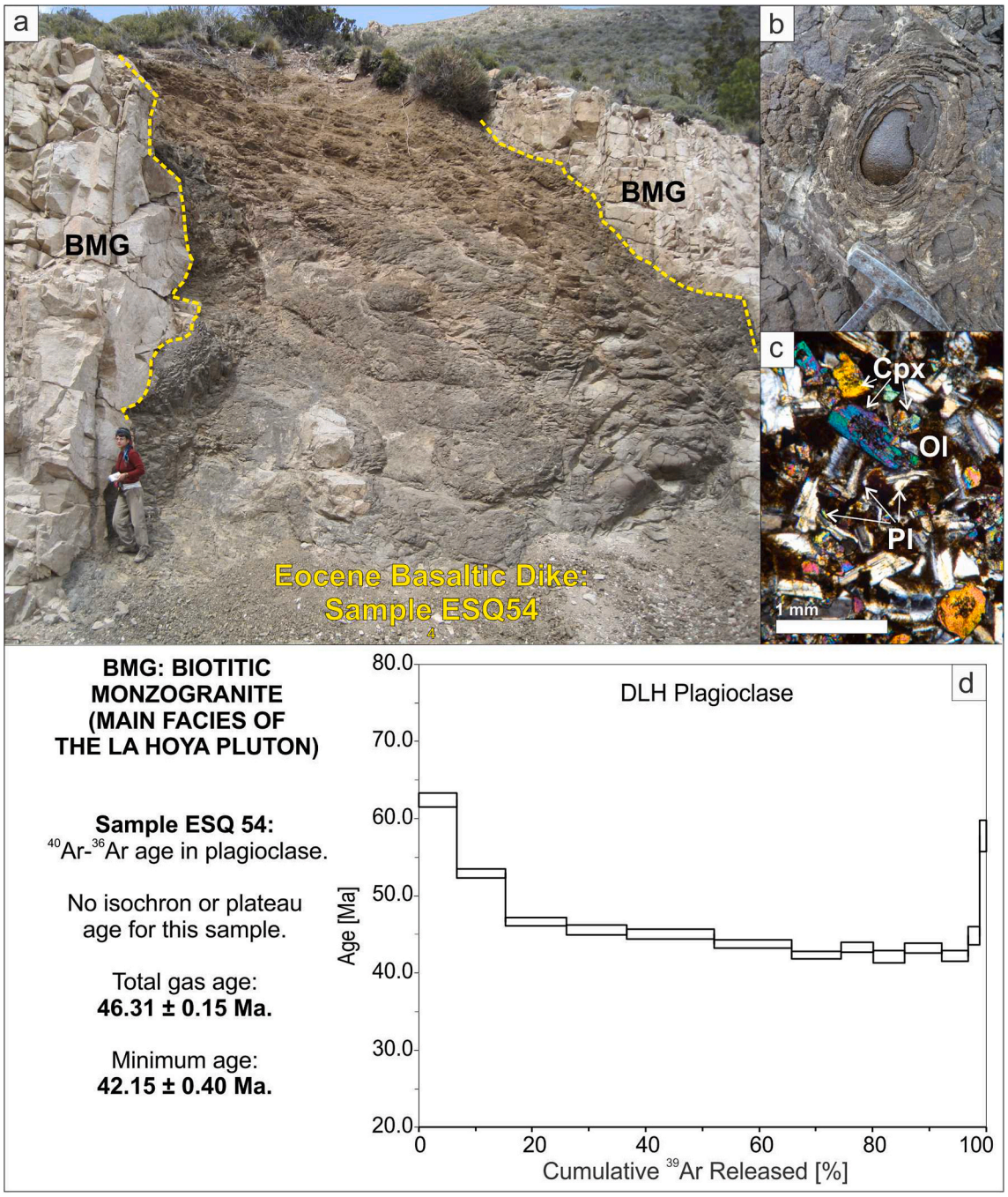

Fig. 9. Eocene basaltic dikes intruding the La Hoya Pluton. a) General view of the subvertical dikes with irregular borders and cataphyllary erosion. b) Detail of the cataphyllary erosion. c) Thin section showing olivine, clinopyroxene and plagioclase phenocrysts. Mineral abbreviation following Whitney and Evans (2010). d) ^{40}Ar-^{39}Ar plateau age from single mineral grains of plagioclase from the basaltic dikes.

2010, Figs. 3a and 11a). This is because the original magmatic foliation, at the emplacement level, is flat or shallowly dipping (Figs. 3a and 8a). The roof of the intrusion, well preserved in the Cordón de Esquel, is flat (Fig. 4a). The host rock at the top of the intrusion (the Esquel/Valle Chico formations in site LH1; Fig. 8i), shows an S0//S1 low-grade metamorphic foliation of subhorizontal attitude. At the roofs and sides of the intrusion, the margins of the growing magma chamber were removed via stoping or diking (Fig. 3a). The magmatic foliation preserved in site LH15, with an unmodified granophyric texture (Fig. 4a), is also subhorizontal (Fig. 8a), probably reflecting its closeness to the pluton roof.

The emplacement of the La Hoya Pluton took place in the Late Jurassic, at 161.9 ± 0.46 Ma Ma (Boltshauser et al., 2019), during a time of tectonic quiescence before the first deformational event of the North Patagonian fold and thrust belt (Somoza and Zaffarana, 2008; Orts et al., 2012; Echaurren et al., 2016, 2017, Fig. 11b). The shallow crustal level of emplacement of the La Hoya Pluton, which implies fast cooling rates, probably preserved the evidence of emplacement as multiple magma pulses, despite the pervasive regional deformation which overprinted the originally magmatic fabric patterns of this pluton in some localities. The amalgamation of the La Hoya Pluton as resulting from different pulses is suggested by its broad compositional range comprised by gabbros, tonalites, granodiorites and monzogranites. The presence of enclave swarms (Fig. 6a-c) also corroborates the amalgamated and

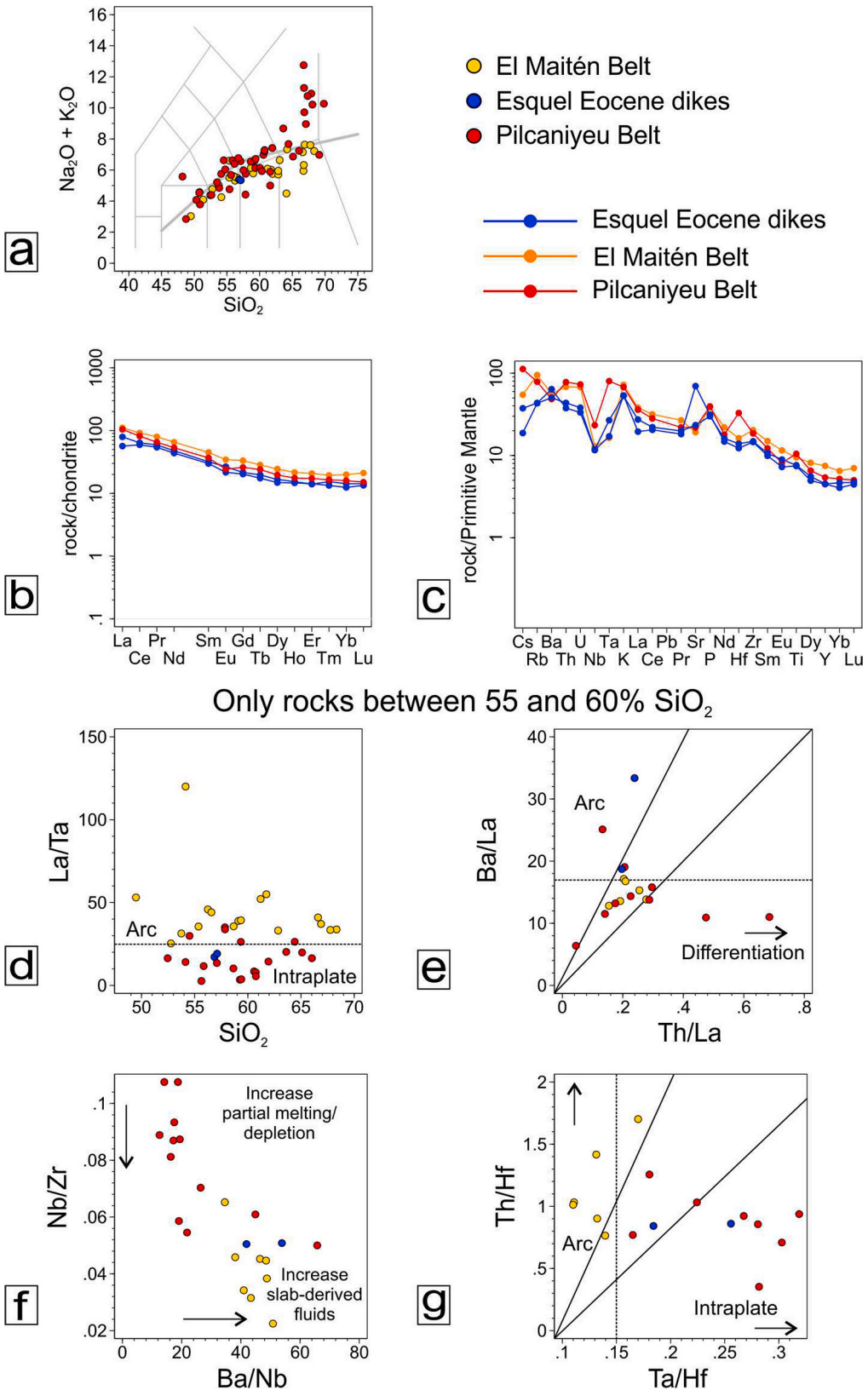

Fig. 10. General geochemical classification of the Eocene basaltic dikes intruding the La Hoya Pluton and its comparison with the Pilcaniyeu (Rapela et al., 1988; Aragón et al., 2011; Iannelli et al., 2017) and the El Maitén (Rapela et al., 1988; Iannelli et al., 2017; Fernández Paz et al., 2018) belts. a) Total alkalis versus silica (TAS) diagram with classification of the studied rocks. Alkaline-subalkaline dividing line after Irvine and Baragar (1971). b) REE pattern of the analyzed rocks normalized to chondrite. c) Primitive Mantle normalized multi-elemental plot. d) Plot of La/Ta vs. SiO_2 e) Ba/La v. Th/La. f) Plot of Nb/Zr v. Ba/Nb. g) Plot of Th/Hf vs. Ta/Hf. Chondrite normalization is from McDonough and Sun (1995) and Primitive Mantle normalization is from Sun and McDonough (1989).

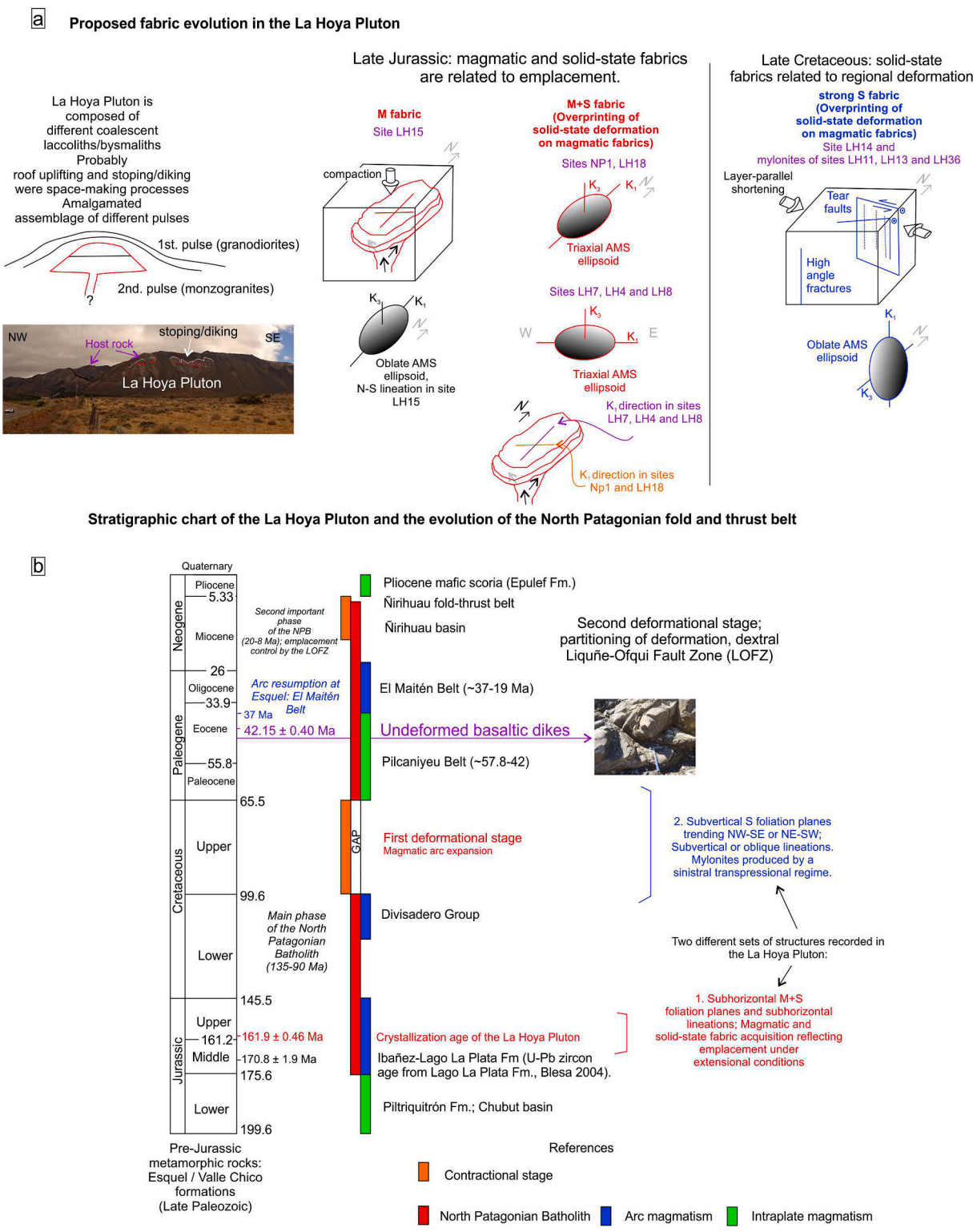

Fig. 11. Discussion of the obtained data. a) Proposed fabric evolution for the La Hoya Pluton. b) The cooling and tectonic overprinting of the La Hoya Pluton in the context of the evolution of the North Patagonian fold and thrust belt.

progressive assemblage of this intrusion as distinct magma pulses. The shallowly dipping magmatic foliation found in the enclave swarms (Fig. 6a; 8g-h) suggests that the La Hoya Pluton experienced sub-horizontal magma flow, as enclave swarms are usually interpreted as conduit feeders, thus original directions of magma flow (Tobisch et al., 1997; Collins et al., 2006). Therefore, the La Hoya Pluton would have had subhorizontal conduits, such as the tube-shaped subhorizontal conduits described as feeders of the laccoliths and bysmaliths from the Henry Mountains by Horsman et al. (2010). Besides, the presence of prolate AMS ellipsoids with steeply plunging lineations in the case of site LH5 from the gabbros and quartz-monzodiorites (Fig. 8d) could point to directions of subvertical magma flow.

The integrated study of field and AMS data together with the deformation microstructures provide timing relationships between

structures found in the La Hoya Pluton, where two different sets of penetrative solid-state structures were recognized. On one side, the presence of shallowly dipping foliation planes could be ascribed to the expression of emplacement conditions, developing during pluton cooling. The associated tectonic lineations, especially in the sites showing a well-developed low-temperature solid-state deformation, are horizontal, having either N–S (site NP1, LH18) or E-W strike (site LH7, LH4, LH8). These directions coincide with the maximum length of the intrusion (N–S) and with the perpendicular direction (E-W) (Fig. 11a). A similar pattern of subhorizontal magmatic and solid-state fabrics was found by Horsman et al. (2010) in the Maiden Creek upper crustal intrusion in the Henry Mountains, USA. The plutons analyzed by the latter authors were emplaced after the peak of the Laramide orogeny during an extensional regime, in Middle to Late Eocene times (from 30 Ma to 21 Ma, Nelson et al., 1992).

In the La Hoya Pluton, sites with subhorizontal foliations developed under solid-state conditions, and show high- and low-temperature solid-state deformation microstructures. Myrmekites, microcline instead of orthoclase and chessboard texture in quartz represent the high-temperature solid-state deformation microstructures in the sites of La Hoya Pluton bearing subhorizontal magnetic foliation planes, whereas low-temperature deformation microstructures are represented by aggregates of quartz and feldspar subgrains which are not still organized in subgrain bands. In summary, subhorizontal fabrics in the La Hoya Pluton developed progressively during cooling and emplacement, first in the magmatic stage and later during high- and low-temperature solid-state conditions. In sites LH8 and LH18, the AMS ellipsoids can be separated into AMS ellipsoids recording a higher and a lower deformation rate. When this separation is made, the M + S and the S ellipsoids still record the same axes K_1, K_2 and K_3 orientations (Table 1, Fig. 8b, h).

If the La Hoya Pluton was deformed in solid-state conditions during cooling, then this deformation should have happened in Late Jurassic times, because fast cooling conditions are inferred from the shallow emplacement level of this pluton.

The main deformational stages in the 41°-44° S sector of the North Patagonian Andes were recognized by several studies and are summarized in Fig. 11b (Giacosa and Heredia, 2004; Somoza and Zaffarana, 2008; Orts et al., 2012, 2015; Encinas et al., 2013, 2014; Bechis et al., 2014; Savignano et al., 2016; Echaurren et al., 2016, 2017; Zaffarana et al., 2018). The first contractional stage occurring in Late Cretaceous times inverted the Jurassic-Lower Cretaceous half-graben systems, reactivating the western Cañadón Asfalto rift border ca. 500 km away from the trench, at a time of arc foreland expansion. In this context, we infer that the original magmatic fabrics of the La Hoya Pluton were modified by regional deformation affecting the North Patagonian Andes. Thus, the presence of subvertical foliation planes in sites LH14, together with the mylonites recorded in sites LH13, LH11 and LH36, as well as the steeply plunging lineations of these deformed rocks, suggest that they represent tear faults, compatible with the E-W compressive tectonic regime prevailing since Late Cretaceous times (Echaurren et al., 2016, 2017 and references therein). The presence of solid-state vertical and intermediate lineations, together with the predominance of subvertical oblate ellipsoids (Fig. 5f and g) is compatible with a local transpressive strike-slip regime (Fossen et al., 1994; Tikoff and Greene, 1997; Fossen and Tikoff, 1998; Saint Blanquat et al., 1998). A transpressive deformation regime was also described in Late Cretaceous times (110-80 Ma), compatible with the development of low-grade shear zones in the North Patagonian Andes by Oriolo et al. (2019).

The E-W trending, horizontal shortening direction inferred from the fabric observed in the Valle Chico Fm. and the subvertical S fabrics of La Hoya Pluton is compatible with a layer parallel shortening, which is an expression of compressive strain that occurs parallel to bedding surfaces (e.g., Weil and Yonkee, 2012). These solid-state deformational microstructures may represent layer-parallel shortening structures, even though this kind of structures were initially described in sedimentary rocks, such as shales and red beds (Weil and Yonkee, 2012) and not in plutonic rocks. However, it has also been described in gneisses and granulites (Kisters et al., 1996). Layer-parallel shortening deformation is typical of early strain and stress patterns in many orogenic belts (e.g., Geiser and Engelder, 1983; Geiser, 1988; Mitra, 1994; Gray and Stamatakos, 1997; Hogan and Dunne, 2001; Ong et al., 2007; Weil and Yonkee, 2012).

Neogene shortening in the North Patagonian Andes has been estimated as 11 km in a 217.65 km length section, representing only a 3.78% of the initial length (Echaurren et al., 2016). This shortening is considerably lower than in the Central Andes to the north (Ramos et al., 2004; Oncken et al., 2006). However, Echaurren et al. (2016) suggested that this is considered a minimum shortening, given that essential sectors of the profile could not be observed in detail. It is possible that the compressive tectonic deformation structures in the Late Jurassic La Hoya Pluton may have been produced by some layer-parallel deformation absorbed by the pluton during the early stages of deformation of the fold and thrust belt.

After the Late Cretaceous deformational stage, the Pilcaniyeu Belt was extruded, representing a flare-up magmatic event coinciding with the collision of the Farallón-Aluk ridge with the South American border (Aragón et al., 2011, 2013; Iannelli et al., 2020). The magmatic and solid-state deformation described in the La Hoya Pluton occurred before the intrusion of the Eocene undeformed basaltic dikes (Fig. 8a–c; 10b). Interestingly, the importance of the Late Cretaceous contractional deformation stage was also highlighted by water isotope studies in the Patagonian Andes, which postulate that their topography was as high as nowadays since at least Paleocene times, and most probably since the Late Cretaceous (Colwyn et al., 2019). Even though we do not discuss their paleo-altitude data, our structural and AMS data are consistent with an early Cenozoic extensional regime and magmatism before Neogene contraction (Colwyn et al., 2019).

The reverse NE-SW trending faults found in site LH11 (Fig. 5h and i) which crosscut the structures formed during the ~E-W directed Cretaceous contraction, are not compatible with the strain ascribed to Late Cretaceous times (Fig. 10a). These faults would belong to a much younger compressive stage, as they crosscut the structures formed during the previous, Late Cretaceous event (field evidence shown in Fig. 5h and i). These faults could have been formed during the second deformational stage of the North Patagonian fold and thrust belt, which occurred since Miocene times due to the growth of the North Patagonian fold-thrust belt (Fig. 10b; Bilmes et al., 2013; Echaurren et al., 2016; D'Elia et al., 2020). Similar NE-SW trending thrusts are seen in the northern part of the Esquel range, in the area between Esquel and Leleque in Fig. 1 and had been mapped previously by Lizuaín and Viera (2010) and by Orts et al. (2012).

6. Conclusions

The AMS and structural study of the La Hoya Pluton reveals that it records magmatic and solid-state deformation textures that are compatible with the deformational stages of this sector of the North Patagonian Andes.

The La Hoya Pluton registers subhorizontal magmatic foliations and shallowly dipping, flattened enclave swarms, which suggest that the pluton was formed by several amalgamated pulses. The La Hoya Pluton was emplaced in Late Jurassic times during a period of relative tectonic quiescence along the Southern Gondwana margin. The subhorizontal magmatic fabrics were partially overprinted by subparallel solid-state deformational fabrics, which developed during fast pluton cooling in Late Jurassic times. Later, NE and NW trending high-angle fractures and mylonites developed, reflecting an E-W shortening direction active in Late Cretaceous times. These mylonites were developed under low-temperature solid-state conditions, and the combination of oblate subvertical magnetic ellipsoids with subvertical lineations is compatible with a transpressive deformational regime. This compressive stress field described here probably took place during the Late Cretaceous

deformation stage, which resulted in the deformation of the North Patagonian fold and thrust belt.

These deformational events occurred before the intrusion of the Eocene basaltic dikes, which have an ^{40}Ar-^{39}Ar crystallization age in plagioclase of 42.15 ± 0.40 Ma and which were ascribed to the early stages of the El Maitén Belt. These dikes have geochemical features coherent with the transition from the alkaline-like geochemical signature with limited slab influence of the Pilcaniyeu Belt to the slab-derived calc-alkaline magmas of the El Maitén Belt.

Finally, a NE-SW trending fault with intermediate inclination towards the SW, and a reverse sense of shear was ascribed to the Miocene deformational stage in the North Patagonian fold and thrust belt. Their relationship with the undeformed Eocene basaltic dikes could not be observed in the field.

Declaration of competing interest

The authors declare that they have no known competing financial interests or personal relationships that could have appeared to influence the work reported in this paper.

Acknowledgements

This work was financed with PIP CONICET 112-200901-00766, PICT 2014–1394, and projects PI-40A-631 and PI-40A-798 from the Universidad Nacional de Río Negro. Guest Editor César Navarrete is thanked for the editorial handling of the manuscript, as well as Dr. Lucas Fennell and an anonymous reviewer for their valuable and constructive comments.The authors also want to thank María Cecilia Ubaldón from the Servicio Geológico Minero Argentino, as well as Dra. Stella Poma from the Buenos Aires University for their help during fieldwork and also for the interesting discussions that we maintained. Lucía Martin is also thanked for her her assistance and companionship during fieldwork.

Appendix A. Supplementary data

Supplementary data to this article can be found online at https://doi.org/10.1016/j.jsames.2020.102791.

Author statement

All persons who meet **authorship** criteria are listed as **authors**, and all **authors** certify that they have participated sufficiently in the work to take public responsibility for the content, including participation in the concept, design, analysis, writing, or revision of the manuscript.

References

Aguirre, L., Cortés, J., Morata, D., Hervé, F., 1997. Low-grade metamorphism of mesozoic and cenozoic volcanic sequences of patagonia, Chile (43-46°S). Rev. Geol. Chile 24, 187–201.

Aragón, E., D' Eramo, F., Castro, A., Pinotti, L., Brunelli, D., Rabbia, O., Cavarozzi, C.E., 2011. Tectono-magmatic response to major convergence changes in the North Patagonian suprasubduction system; the Paleogene subduction–transcurrent plate margin transition. Tectonophysics 509 (3–4), 218–237.

Aragón, E., Pinotti, L., Eramo, F.D., Castro, A., Rabbia, O., Coniglio, J., Demartis, M., Hernando, I., Cavarozzi, C.E., Aguilera, Y.E., 2013. Geoscience Frontiers the Farallon-Aluk ridge collision with South America: implications for the geochemical changes of slab window magmas from fore- to back-arc. Geoscience Frontiers 4 (4), 377–388. https://doi.org/10.1016/j.gsf.2012.12.004.

Archanjo, C.J., Launeau, P., Bouchez, J.L., 1995. Magnetic fabric vs. magnetite and biotite shape fabrics of the magnetite-bearing granite pluton of Gameleiras (Northeast Brazil). Phys. Earth Planet. In. 89, 63–75. https://doi.org/10.1016/0031-9201(94)02997-P.

Archanjo, C.J., Trindade, R.I.F., Bouchez, J.L., Ernesto, M., 2002. Granite fabrics and regional-scale strain partitioning in the Seridó belt (Borborema Province, NE Brazil). Tectonics 21, 3–14. https://doi.org/10.1029/2000TC001269.

Bechis, F., Cristallini, E.O., 2006. Inflexiones en estructuras del sector norte de la faja plegada y corrida de Nirihuau, provincia de Río Negro. Rev. Asoc. Geol. Argent. 25, 18–25.

Bechis, F., Encinas, A., Concheyro, A., Litvak, V.D., Aguirre-Urreta, B., Ramos, V.A., 2014. New age constraints for the Cenozoic marine transgressions of northwestern Patagonia, Argentina (41°-43°S): paleogeographic and tectonic implications. J. S. Am. Earth Sci. 52, 72–93.

Bilmes, A., D' Elia, L., Franzese, J.R., Veiga, G.D., Hernández, M., 2013. Miocene block uplift and basin formation in the Patagonian foreland: the Gastre Basin, Argentina. Tectonophysics 601, 98–111. https://doi.org/10.1016/j.tecto.2013.05.001.

Blesa, A., 2004. Geology and Mineralization of the Esquel Area, Patagonia Argentina. MsSc. thesis. Colorado School of Mines.

Blumenfeld, P., Mainprice, D., Bouchez, J.L., 1986. C-slip in quartz from subsolidus deformed granite. Tectonophysics 127, 97–115.

Boltshauser, B., Zaffarana, C.B., Gallastegui, G., Orts, D., Poma, S., Serra Varela, S., Ruiz González, V., 2019. Caracterización petrológica del Plutón de La Hoya, Jurásico Medio a Superior del Batolito Patagónico en Esquel. XIII MinMet - IV PIMMA. Actas, Córdoba, Argentina, pp. 47–48.

Borradaile, G.J., Henry, B., 1997. Tectonic applications of magnetic susceptibility and its anisotropy. Earth Sci. Rev. 42, 49–93. https://doi.org/10.1016/S0012-8252(96)00044-X.

Borradaile, G.J., Jackson, M., 2010. Structural geology, petrofabrics and magnetic fabrics (AMS, AARM, AIRM). J. Struct. Geol. 32 (10), 1519–1551.

Bouchez, J.L., 2000. Anisotropie de susceptibilite magnetique et fabrique des granites. Comptes Rendus l'Academie Sci - Ser IIa Sci la Terre des Planetes. 330, 1–14. https://doi.org/10.1016/S1251-8050(00)00120-8.

Bouchez, J.L., Delas, C., Gleizes, G., Nédélec, A., Cuney, M., 1992. Submagmatic microfractures in granites. Geology 20, 35–38.

Bruce, R.M., Nelson, E.P., Weaver, S.G., Lux, D.R., 1991. Temporal and spatial variation in the southern Patagonian Batholith: constraints on magmatic arc development. In: Harmon, R.S., Rapela, C.W. (Eds.), Andean Magmatism and its Tectonic Setting. Special Paper, vol. 265. Geological Society of America, pp. 1–12.

Castro, A., Moreno-Ventas, I., Fernández, C., Vujovich, G., Gallastegui, G., Heredia, N., Martino, R.D., Becchio, R., Corretgé, L.G., Díaz-Alvarado, J., Such, P., García-Arias, M., Liu, D.-Y., 2011. Petrology and SHRIMP U-Pb zircon geochronology of Cordilleran granitoids of the Bariloche area, Argentina. J. S. Am. Earth Sci. 32 (4), 508–530. https://doi.org/10.1016/j.jsames.2011.03.011.

Cazau, L., 1972. Cuenca de Nirihuau-Norquincó-Cushamen. In: Leanza, A.F. (Ed.), Geología Regional Argentina. Academia Nacional de Ciencias de Córdoba, pp. 727–740.

Chadima, M., Jelinek, V., 2008. Anisoft 4.2, Anisotropy Data Browser for Windows. www.agico.com.

Charrier, R., Baeza, O., Elgueta, S., Flynn, J., Gans, J., Kay, S.M., Muñoz, N., Wyss, A.R., Zurita, E., 2002. Evidence for Cenozoic extensional basin development and tectonic inversion south of the flat-slab segment, southern Central Andes, Chile (33°–36° S. L.). J. S. Am. Earth Sci. 15, 117–139.

Collins, W.J., Wiebe, R.A., Healy, B., Richards, S.W., 2006. Replenishment, crystal accumulation and floor aggradation in the megacrystic Kameruka Suite, Australia. J. Petrol. 47, 2073–2104. https://doi.org/10.1093/petrology/egl037.

Colwyn, D.A., Brandon, M.T., Hren, M.T., Hourigan, J., Pacini, A., Cosgrove, M.G., Midzik, M., Garreaud, R.D., Metzger, C., 2019. Growth and steady state of the patagonian Andes. Am. J. Sci. 319, 431–472. https://doi.org/10.2475/06.2019.01.

Dalla Salda, L., Leguizamón, M., Mazzoni, M., Merodio, J., Rapela, C., Spalletti, L., 1981. Características del vulcanismo paleógeno de la Cordillera Nordpatagónica entre las latitudes 39°30' y 41°20'S. 8° Congreso Geológico Argentino, vol. 3. Actas, pp. 629–657.

D'Elia, L., Bilmes, A., Varela, A.M., Bucher, J., López, M., García, M., Ventura Santos, R., Hauser, N., Naipauer, M., Sato, A.M., Franzese, J., 2020. Geochronology, sedimentology and paleosol analysis of a Miocene, syn-orogenic, volcaniclastic succession (La Pava Formation) in the north Patagonian foreland: tectonic, volcanic and paleoclimatic implications. J. S. Am. Earth Sci. 100 https://doi.org/10.1016/j.jsames.2020.102555.

D'Eramo, F., Pinotti, L., Tubia, J.M., Vegas, N., Aranguren, A., Tejero, R., Gómez, D., 2006. Coalescence of lateral spreading magma ascending through dykes: a mechanism to form a granite canopy (El Hongo pluton, Sierras Pampeanas, Argentina). Journal of the Geological Society of London 163, 881–892. https://doi.org/10.1144/0016-764905-060.

Day, R., Fuller, M., Schmidt, V.A., 1977. Hysteresis properties of titanomagnetites: grain-size and compositional dependence. Phys. Earth Planet. In. 13, 260–267. https://doi.org/10.1016/0031-9201(77)90108-X.

Echaurren, A., Folguera, A., Gianni, G., Orts, D., Tassara, A., Encinas, A., Gimenez, A., Valencia, V., 2016. Tectonic evolution of the North Patagonian Andes (41–44 S) through recognition of syntectonic strata. Tectonophysics 677, 99–114.

Echaurren, A., Oliveros, V., Folguera, A., Ibarra, F., Creixell, C., Lucassen, F., 2017. Early Andean tectonomagmatic stages in north Patagonia: insights from field and geochemical data. Journal of the Geological Society of London 174 (3), 405–421. https://doi.org/10.1144/jgs2016-087.

Eggleton, R.A., Buseck, P.R., 1980. The orthoclase-microcline inversion: a high-resolution transmission electron microscope study and strain analysis. Contrib. Mineral. Petrol. 74, 123–133.

Encinas, A., Zambrano, P.A., Finger, K.L., Valencia, V., Buatois, L.A., Duhart, P., 2013. Implications of deep-marine Miocene deposits on the evolution of the north patagonian Andes. J. Geol. 121, 215–238.

Encinas, A., Pérez, F., Nielsen, S.N., Finger, K.L., Valencia, V., Duhart, P., 2014. Geochronologic and paleontologic evidence for a pacific–atlantic connection during the late oligocene–early Miocene in the patagonian Andes (43–44° S). J. S. Am. Earth Sci. 55, 1–18.

Fernández Paz, L., Litvak, V.D., Echaurren, A., Iannelli, S.B., Encinas, A., Folguera, A., Valencia, V., 2018. Late Eocene volcanism in North Patagonia (42°30'-43°S): arc resumption after stage of within-plate magmatism. J. Geodyn. 113, 13–31.

Fernández Paz, L., Bechis, F., Litvak, V.D., Echaurren, A., Encinas, A., González, J., Lucassen, F., Oliveros, V., Valencia, V., Folguera, A., 2019. Constraints on trenchward arc migration and backarc magmatism in the north patagonian Andes in the context of nazca plate rollback. Tectonics 38, 3794–3817. https://doi.org/10.1029/2019TC005580.

Fernández Paz, L., Iannelli, S.B., Echaurren, A., Ramos, M., Bechis, F., Litvak, V., Encinas, A., Kasemann, S., Lucassen, F., Folguera, A., 2020. The late Eocene–early Miocene El Maitén Belt evolution: magmatic response to the changing subduction zone geodynamics. J. S. Am. Earth Sci. 103, 102713. https://doi.org/10.1016/j.jsames.2020.102713.

Ferré, E.C., Améglio, L., 2000. Preserved magnetic fabrics vs annealed microstructures in the syntectonic recrystallised George granite, South Africa. J. Struct. Geol. 22, 1199–1219.

Feruglio, E., 1949. Descripción geológica de la Patagonia. Dirección General de Yacimientos Petrolíferos Fiscales, 3 tomos, T1: 1-323; T2: 1-349; T3: 1-331. Buenos Aires. http://www.insugeo.org.ar/publicaciones/docs/scg-24-0-16.pdf.

Fossen, H., Tikoff, B., 1998. Extended models of transpression and transtension, and application to tectonic settings. In: Holdsworth, R.E., Strachan, R.A., Dewey, J.F. (Eds.), Continental Transpressional and Transtensional Tectonics, vol. 135. Geological Society of London Special Publication, pp. 15–33. https://doi.org/10.1144/GSL.SP.1998.135.01.02.

Fossen, H., Tikoff, B., Teyssier, C., 1994. Strain modeling of transpressional and transtensional deformation. Nor. Geol. Tidsskr. 74, 134–145.

Geiser, P.A., 1988. Mechanisms of thrust propagation; some examples and implications for the analysis of overthrust terranes. J. Struct. Geol. 10, 829–845.

Geiser, P.A., Engelder, T., 1983. The distribution of layer parallel shortening fabrics in the Appalachian foreland of New York and Pennsylvania; evidence for two non-coaxial phases of the Alleghanian orogeny. In: Hatcher Jr., R.D. (Ed.), Contributions to the Tectonics and Geophysics of Mountain Chains, vol. 158. Geological Society of America, Memoirs, pp. 161–175.

Giacosa, R., Heredia, N., 2004. Structure of the North Patagonian thick-skinned fold-and-thrust belt, southern central Andes, Argentina (41°–42°S). J. S. Am. Earth Sci. 18 (1), 61–72. https://doi.org/10.1016/j.jsames.2004.08.006.

Godoy, E., Yáñez, G., Vera, E., 1999. Inversion of an Oligocene volcano-tectonic basin and uplifting of its superimposed Miocene magmatic arc in the Chilean Central Andes: first seismic and gravity evidences. Tectonophysics 306, 217–236.

González Bonorino, G., 1974. La Formación Millaqueo y la "Serie Porfírica" de la Cordillera Nordpatagónica: nota preliminar. Rev. Asoc. Geol. Argent. 29 (3), 145–154.

González Bonorino, G., 1992. Carboniferous glaciation in Gondwana. Evidence for grounded marine ice and continental glaciation in southwestern Argentina. Palaeogeogr. Palaeoclimatol. Palaeoecol. 91, 363–375.

Gray, M.B., Stamatakos, J., 1997. New model for evolution of fold and thrust belt curvature, based on integrated structural and paleomagnetic results from the Pennsylvania salient. Geology 25, 1067–1070.

Gordon, A., Ort, M.H., 1993. Edad y correlación del plutonismo subcordillerano en las provincias de Río Negro y Chubut (41°-42° 30'LS). In: XII Congreso Geológico Argentino y II Congreso de Exploración de Hidrocarburos, pp. 120–127.

Haller, M.J., Linares, E., Ostera, H., Page, S., 1999. Petrology and Geochronology of the Sub-cordilleran Plutonic Belt of Patagonia. II South American Symposium on Isotope Geology, Carlos Paz, Argentina. Segemar, Buenos Aires, pp. 210–214.

Haller, M., Lapido, O.R., 1982. The jurassic-cretaceous volcanism in the septentrional patagonian Andes. Earth Sci. Rev. 18 (3–4), 395–410. https://doi.org/10.1016/0012-8252(82)90046-0. ISSN 0012-8252.

Higgins, M.D., 2011. Textural coarsening in igneous rocks. Int. Geol. Rev. 53 (3–4), 37–41. https://doi.org/10.1080/00206814.2010.496177.

Hogan, J.P., Dunne, W.M., 2001. Calculation of shortening due to outcrop-scale deformation and its relation to regional deformation patterns. J. Struct. Geol. 23, 1508–1529.

Horsman, E., Morgan, S., Blanquat, M.D., Saint Habert, G., Nugent, A., Hunter, R.A., Tikoff, B., 2010. Emplacement and assembly of shallow intrusions from multiple magma pulses, Henry Mountains, Utah. Earth and Environmental Science Transactions of the Royal Society of Edinburgh 100, 117–132. https://doi.org/10.1017/S1755691009016089.

Iannelli, S., Fernández Paz, L., Litvak, V.D., Gianni, G., Fennell, L., Gonzalez, J., Oliveros, V., Folguera, A., Lucassen, F., 2020. Southward-directed Subduction of the Farallon-Aluk Spreading Ridge and its Impact on Subduction Mechanics and Andean Arc Magmatism: Insights from Geochemical and Seismic Tomographic Data. Frontiers in Earth Sciences. https://www.frontiersin.org/article/10.3389/feart.2020.00121; DOI=10.3389/feart.2020.00121.

Iannelli, S., Litvak, V.D., Fernández Paz, L., Folguera, A., Ramos, M.E., Ramos, V.A., 2017. Evolution of Eocene to oligocene arc-related volcanism in the north patagonian Andes (39-41°S), prior to the break-up of the farallon plate. Tectonophysics 696–697, 70–87.

Irvine, T.N., Baragar, W.R.A., 1971. A guide to the chemical classification of the common volcanic rocks. Can. J. Earth Sci. 8, 523–548.

Jelinek, V., 1978. Statistical processing of anisotropy of magnetic susceptibility measured on groups of specimens. Studia Geophysica et Geodetica 22, 50–62. https://doi.org/10.1007/BF01613632.

Jelinek, V., 1981. Characterization of the magnetic fabric of rocks. Tectonophysics 79, 63–67.

Jordan, T.E., Burns, W.M., Veiga, R., Pángaro, F., Copeland, P., Kelley, S., Mpodozis, C., 2001. Extension and basin formation in the southern Andes caused by increased convergence rate: a mid-Cenozoic trigger for the Andes. Tectonics 20 (3), 308–324. https://doi.org/10.1029/1999TC001181.

Kisters, A.F.M., Guy Charlesworth, E., Gibson, R.L., Anhaeusser, C.R., 1996. Steep structure formation in the Okiep Copper District, South Africa: bulk inhomogeneous shortening of a high-grade metamorphic granite-gneiss sequence. J. Struct. Geol. 18 (6), 735–751.

Le Bas, M.J., Lemaître, R.W., Streckeisen, A., Zanettin, B., 1986. A chemical classification of volcanic rocks based on the total alkali-silica diagram. J. Petrol. 27, 745–750.

Litvak, V.D., Encinas, A., Oliveros, V., Bechis, F., Folguera, A., Ramos, V.A., 2014. El volcanismo mioceno inferior vinculado a las ingresiones marinas en los Andes Nordpatagónicos. 19° Congreso Geológico Argentino, Actas S22-35, Córdoba.

Lizuaín, A., 1980. Las formaciones suprapaleozoicas y jurásicas de la Cordillera patagónica. Provincias de Río negro y chubut. Rev. Asoc. Geol. Argent. 25 (2), 174–182.

Lizuaín, A., 2010. Hoja Geológica 4372-I Y II 1:250.000 Esquel. Boletín N 369. Servicio Geológico Minero Argentino, p. 72.

Lizuaín, A., Viera, R.M., 2010. Descripción Geológica de La Hoja 4372-I y II, Esquel, Provincia de Chubut. Secretaría de Minería, Dirección Nacional del Servicio Geológico, Buenos Aires.

Mainprice, D., Bouchez, J.L., Blumenfeld, P., Tubia, J.M., 1986. Dominant c-slip in naturally deformed quartz: implications for drastic plastic softening at high temperature. Geology 14, 819–822.

McDonough, W.F., Sun, S.S., 1995. The composition of the Earth. Chem. Geol. 120, 223–253.

McNulty, B.A., Tobisch, O.T., Cruden, A.R., Gilder, S., 2000. Multistage emplacement of the mount givens pluton, central sierra Nevada batholith, California. Bull. Geol. Soc. Am. 112, 119–135. https://doi.org/10.1130/0016-7606(2000)112<119:MEOTMG>2.0.CO;2.

Massaferro, G., 2000. Metamorphic and alteration proceses in a jurassic sequence from the central patagonian cordillera, chubut. Rev. Asoc. Geol. Argent. 55, 291–299.

Mitra, G., 1994. Strain variation in thrust sheets across the Sevier fold-and-thrust belt (Idaho-Utah-Wyoming); implications for section restoration and wedge taper evolution. J. Struct. Geol. 16, 585–602.

Munizaga, F., Hervé, F., Drake, R., Pankhurst, R., Brook, M., Snelling, N., 1988. Geochronology of the lake region of south-central Chile (39– 42 S): preliminary results. J. S. Am. Earth Sci. 1 (3), 309–316. https://doi.org/10.1016/0895-9811(88)90009-0.

Nédélec, A., Bouchez, J.-L., 2015. Granites: Petrology, Structure, Geological Setting, and Metallogeny, 1 edition. OUP, Oxford.

Nelson, S.T., Davidson, J.P., Sullivan, K.R., 1992. New age determinations of central Colorado Plateau laccoliths, Utah: recognizing disturbed K–Ar systematics and re-evaluating tectonomagmatic relationships. Geol. Soc. Am. Bull. 104, 1547–1560.

Neves, S.P., Araújo, A.M.B., Correia, P.B., Mariano, G., 2003. Magnetic fabrics in the Cabanas Granite (NE Brazil): interplay between emplacement and regional fabrics in a dextral transpressive regime. J. Struct. Geol. 25, 441–453. https://doi.org/10.1016/S0191-8141(02)00003-2.

Olivier, P., Druguet, E., Castaño, L.M., Gleizes, G., 2015. Granitoid emplacement by multiple sheeting during Variscan dextral transpression: the Saint-Laurent - La Jonquera pluton (Eastern Pyrenees). J. Struct. Geol. 82, 80–92. https://doi.org/10.1016/j.jsg.2015.10.006.

Oncken, O., Hindle, D., Kley, J., Elger, K., Victor, P., Schemmann, K., 2006. Deformation of the central Andean upper plate system—facts, fiction, and constraints for plateau models. In: Oncken, et al. (Eds.), The Andes: Active Subduction Orogeny. Springer-Verlag, Berlin, pp. 3–27.

Ong, P.F., van der Pluijm, B.A., van der Voo, R., 2007. Early rotation and late folding in the Pennsylvania Salient (U.S. Appalachians); evidence from calcite-twinning analysis of Paleozoic carbonates. Bull. Geol. Soc. Am. 119, 796–804.

Oriolo, S., Schulz, B., González, P.D., Bechis, F., Olaizola, E., Krause, J., Renda, E., Vizán, H., 2019. The late paleozoic tectonometamorphic evolution of patagonia revisited : insights from the pressure-temperature-deformation-time (P-T-D-t) path of the gondwanide basement of the north patagonian cordillera (Argentina). Tectonics 38 (7), 2378–2400. https://doi.org/10.1029/2018TC005358.

Orts, D.L., Folguera, A., Encinas, A., Ramos, M., Tobal, J., Ramos, V.A., 2012. Tectonic development of the North Patagonian Andes and their related Miocene foreland basin (41° 30′-43° S). Tectonics 31, 1–24. https://doi.org/10.1029/2011TC003084.

Orts, D.L., Folguera, A., Giménez, M., Ruiz, F., Rojas Vera, E.A., Lince Klinger, F., 2015. Cenozoic builiding and deformational processes in the north patagonian Andes. J. Geodyn. 86, 26–41. https://doi.org/10.1016/j.jog.2015.02.002.

Pankhurst, R., Hervé, F., 1994. Granitoid age distribution and emplacement control in the North Patagonian batholith in Aysén (44°-47°). In: Congreso Geológico Chileno, vol. 7. Actas, pp. 1409–1413, 2 (Concepción).

Pankhurst, R.J., Hervé, F., Rojas, L., Cembrano, J., 1992. Magmatism and tectonics in continental Chiloé, Chile. Tectonophysics 205, 283–294.

Pankhurst, R.J., Weaver, S.D., Hervé, F., Larrondo, P., 1999. Mesozoic- cenozoic evolution of the north patagonian batholith in aysen, southern Chile. Journal of the Geological Society of London 156 (4), 673–694. https://doi.org/10.1144/gsjgs.156.4.0673.

Pankhurst, R.J., Rapela, C.W., Fanning, C.M., Márquez, M., 2006. Gondwanide continental collision and the origin of Patagonia. Earth Sci. Rev. 76, 235–257. https://doi.org/10.1016/j.earscirev.2006.02.001.

Parés, J.M., van der Pluijm, B., 2002. Evaluating magnetic lineations (AMS) in deformed rocks. Tectonophysics 350, 283–298.

Passchier, C.W., Trouw, R.A., 2005. Microtectonics. Springer Science & Business Media, p. 366p.

Paterson, S.R., Vernon, R.H., Tobisch, O.T., 1989. A review of criteria for the identification of magmatic and tectonic foliations in granitoids. J. Struct. Geol. 11, 349–363. https://doi.org/10.1016/0191-8141(89)90074-6.

Paterson, S.R., Yoshinobu, A.S., Yuan, E.S., Miller, R.B., Fowler, T.K., Schmidt, K.L., 1998. Interpreting magmatic fabric patterns in plutons. Lithos 44, 53–82. https://doi.org/10.1016/S0024-4937(98)00022-X.

Pryer, L.L., 1993. Microstructures in feldspars from a major crustal thrust zone: the Grenville Front, Ontario, Canada. J. Struct. Geol. 15, 21–36.

Radic, J., Rojas, L., Carpinelli, A., Zurita, E., 2002. Evolución tectónica de la Cuenca Terciaria de Cura Mallín, región cordillerana chileno-Argentina (36°30' –39°S). In: 15th Congreso Geológico Argentino, El Calafate (Electronic Files).

Ramos, V.A., Niemeyer, H., Skarmeta, J., Muñoz, J., 1982. Magmatic evolution of the austral patagonian Andes. Earth Sci. Rev. 18, 411–443.

Ramos, V.A., Zapata, T., Cristallini, E., Introcaso, A., 2004. The Andean thrust system-Latitudinal variations in structural styles and orogenic shortening. In: McClay, K. (Ed.), Thrust Tectonics and Hydrocarbon Systems, vol. 82. AAPG Memoir, pp. 30–50.

Ramsay, J.G., Huber, M.I., 1983. Strain Analysis. In: The Techniques of Modern Structural Geology, vol. 1. Academic Press, London, p. 307.

Rapela, C.W., Spalletti, L.A., Merodio, J., Aragón, E., 1984. El vulcanismo Paleoceno-Eoceno de la provincia volcánica Andino-Patagónica. Relatorio 9° Congreso Geológico Argentino 1 (8), 189–213 (San Carlos de Bariloche).

Rapela, C.W., Spalletti, L.A., Merodio, J.C., Aragón, E., 1988. Temporal evolution and spatial variation of early tertiary volcanism in the Patagonian Andes (40°S-42°30′S). J. S. Am. Earth Sci. 1 (1), 75–88.

Rapela, C.W., Pankhurst, R.J., Fanning, C.M., Herve, F., 2005. Pacific subduction coeval with the Karoo mantle plume: the early Jurassic subcordilleran belt of northwestern Patagonia. Geological society of London, Special Publication 246, 217–239. https://doi.org/10.1144/GSL.SP.2005.246.01.07.

Rochette, P., Jackson, M., Aubourg, C., 1992. Rock magnetism and the interpretation of anisotropy of magnetic susceptibility. Rev. Geophys. 30 (3), 209–226. https://doi.org/10.1029/92RG00733.

Rochette, P., Aubourg, C., Perrin, M., 1999. Is this magnetic fabric normal? A review and case studies in volcanic formations. Tectonophysics 307, 219–234. https://doi.org/10.1016/S0040-1951(99)00127-4.

Rolando, A.P., Hartmann, L.A., Santos, J.O.S., Fernandez, R.R., Etcheverry, R.O., Schalamuk, I.A., McNaughton, N.J., 2002. SHRIMP zircón U-Pb evidence for extended Mesozoic magmatism in the Patagonian Batholith and assimilation of Archean crystal components. J. S. Am. Earth Sci. 15, 267–283.

Saint Blanquat, M., Tikoff, B., 1997. Development of magmatic to solid-state fabrics during syntectonic emplacement of the mono Creek granite, sierra Nevada batholith. In: Bouchez, J., Hutton, D., Stephens, W. (Eds.), Granite: from Segregation of Melt to Emplacement Fabrics, pp. 231–252.

Saint Blanquat, M., Tikoff, B., Teyssier, C., Vigneresse, J.L., 1998. Transpressional kinematics and magmatic arcs. In: Holdsworth, R.E., Strachan, R.A., Dewey, J.F. (Eds.), Continental Transpressional and Transtensional Tectonics, vol. 135. Geological Society of London Special Publication, pp. 327–340. https://doi.org/10.1144/GSL.SP.1998.135.01.21.

Savignano, E., Mazzoli, S., Arce, M., Franchini, M., Gautheron, C., Paolini, M., Zattin, M., 2016. (Un)coupled thrust belt-foreland deformation in the northern Patagonian Andes: new insights from the Esquel-Gastre sector (41° 30'–43° S). Tectonics 35, 2636–2656.

Somoza, R., Zaffarana, C.B., 2008. Mid-Cretaceous polar standstill of South America, motion of the Atlantic hotspots and the birth of the Andean cordillera. Earth Planet Sci. Lett. 271 (1–4), 267–277. https://doi.org/10.1016/j.epsl.2008.04.004.

Somoza, R., Tomlinson, A.J., Zaffarana, C.B., Singer, S.E., Puigdomenech Negre, C.G., Raposo, M.I.B., Dilles, J.H., 2015. Tectonic rotations and internal structure of Eocene plutons in Chuquicamata, northern Chile. Tectonophysics 654, 113–130. https://doi.org/10.1016/j.tecto.2015.05.005.

Stevenson, C., 2009. The relationship between forceful and passive emplacement: the interplay between tectonic strain and magma supply in the Rosses Granitic Complex, NW Ireland. J. Struct. Geol. 31, 270–287. https://doi.org/10.1016/j.jsg.2008.11.009.

Sun, S.S., McDonough, W.F., 1989. Chemical and iso- topic systematics of oceanic basalts: implications for mantle composition and processes. In: Saunders, A.D., Norry, M.J. (Eds.), Magmatism in the Ocean Basins, vol. 42. Geological Society of London, Special Publication, pp. 313–345.

Tikoff, B., Greene, D., 1997. Stretching lineations in transpressional shear zones: an example from the Sierra Nevada Batholith, California. J. Struct. Geol. 19, 29–39. https://doi.org/10.1016/S0191-8141(96)00056-9.

Tobisch, O.T., McNulty, B.A., Vernon, R.H., 1997. Microgranitoid enclave swarms in granitic plutons, central Sierra Nevada, California. Lithos 40, 321–339. https://doi.org/10.1016/S0024-4937.(97)00004-2.

Toubes, R.O., Spikermann, J.P., 1973. Algunas edades K/Ar y Rb/Sr de plutonitas de la Cordillera Patagónica entre los paralelos 40° y 44° de latitud sur. Rev. Asoc. Geol. Argent. 28, 382–396.

Vattuone, M.E., Latorre, C.O., Leal, P.R., 2001. Procesos de formación de paragénesis ceolíticas en el metamorfismo de bajo grado de las volcanitas paleógenas al sur de Confluencia, Neuquén, República Argentina. Rev. Geol. Chile 28 (2), 209–228. https://doi.org/10.4067/S0716-02082001000200004.

Vernon, R.H., 2000. Review of microstructural evidence of magmatic and solid-state flow. Vis. Geosci. Annu. Arch. 5, 1–23. https://doi.org/10.1007/s10069-000-0002-3.

Weil, A.B., Yonkee, W.A., 2012. Layer-parallel shortening across the Sevier fold-thrust belt and Laramide foreland of Wyoming: spatial and temporal evolution of a complex geodynamic system. Earth Planet Sci. Lett. 357–358, 405–420. https://doi.org/10.1016/j.epsl.2012.09.021.

Whitney, D.L., Evans, B.W., 2010. Abbreviations for names of rock-forming minerals. Am. Mineral. 95, 185–187. https://doi.org/10.2138/am.2010.3371.

Zaffarana, C.B., Somoza, R., Orts, D.L., Mercader, R., Boltshauser, B., González, V.R., Puigdomenech, C., 2017. Internal structure of the late triassic central patagonian batholith at gastre, southern Argentina: implications for pluton emplacement and the gastre fault system. Geosphere 13 (6), 1973–1992. https://doi.org/10.1130/GES01493.1.

Zaffarana, C.B., Lagorio, S.L., Orts, D., Busteros, A., Silva Nieto, D., Giacosa, R., Ruiz González, V., Puigdomenech Negre, C., Somoza, R., Haller, M., 2018. First geochemical and geochronological characterization of Late Cretaceous mesosilicic magmatism in Gastre, Northern Patagonia, and its tectonic relation to other coeval volcanic rocks in the region. Geol. Mag. 156 (7), 1285–1294. https://doi.org/10.1017/S0016756818000432.

Zaffarana, C.B., Lagorio, S., Gallastegui, G., Wörner, G., Orts, D., Gregori, D., Poma, S., Busteros, A., Giacosa, R., Silva Nieto, D., Ruiz González, V., Bolsthauser, B., Puigdomenech, C., Haller, M., 2020. Petrogenetic study of the lonco trapial volcanism and its comparison with the early-middle jurassic magmatic units from northern patagonia. J. S. Am. Earth Sci. 101 (102624).

Žák, J., Schulmann, K., Hrouda, F., 2005. Multiple magmatic fabrics in the Sázava pluton (Bohemian Massif, Czech Republic): a result of superposition of wrench-dominated regional transpression on final emplacement. J. Struct. Geol. 27, 805–822. https://doi.org/10.1016/j.jsg.2005.01.012.